Liver proteome profiling in dairy cows during the transition from gestation to lactation: Effects of supplementation with essential fatty acids and conjugated linoleic acids as explored by PLS-DA

Arash Veshkini, Harald M. Hammon, Laura Vogel, Mylène Delosière, Didier Viala, Sèbastien Dèjean, Arnulf Tröscher, Fabrizio Ceciliani, Helga Sauerwein, Muriel Bonnet

Liver proteome profiling in dairy cows during the transition from gestation to lactation: Effects of supplementation with essential fatty acids and conjugated linoleic acids as explored by PLS-DA

Authors:

Arash Veshkini[1,2,3,4], Harald M. Hammon[2*], Laura Vogel[2], Mylène Delosière[3], Didier Viala[3], Sèbastien Dèjean[5], Arnulf Tröscher[6], Fabrizio Ceciliani[4], Helga Sauerwein[1], Muriel Bonnet[3*]

* These authors are co-corresponding authors to this work.

Affiliations:

[1]Institute of Animal Science, Physiology Unit, University of Bonn, Bonn, Germany

[2]Research Institute for Farm Animal Biology (FBN), 18196 Dummerstorf, Germany

[3]INRAE, Université Clermont Auvergne, VetAgro Sup, UMR Herbivores, F-63122 Saint-Genès-Champanelle, France

[4]Department of Veterinary Medicine, Università degli Studi di Milano, Lodi, Italy

[5]Institut de Mathématiques de Toulouse, UMR5219, Université de Toulouse, CNRS, UPS, 31062 Toulouse, France.

[6] BASF SE, 68623 Lampertheim, Germany.

Corresponding authors:

1- Muriel Bonnet (muriel.bonnet@inrae.fr)

2- Harald M. Hammon (hammon@fbn-dummerstorf.de)

1&2 are co-corresponding authors to this work.

Highlights

1. Supplementation with fatty acids affected the liver proteome in dairy cows
2. Out of 1680 proteins identified, 96 were differentially abundant
3. The key pathways involved were Cytochrome P450 and ω-oxidation of fatty acids
4. Specific cytochrome P450 (CYP) enzymes were identified at each time point

Graphical abstract

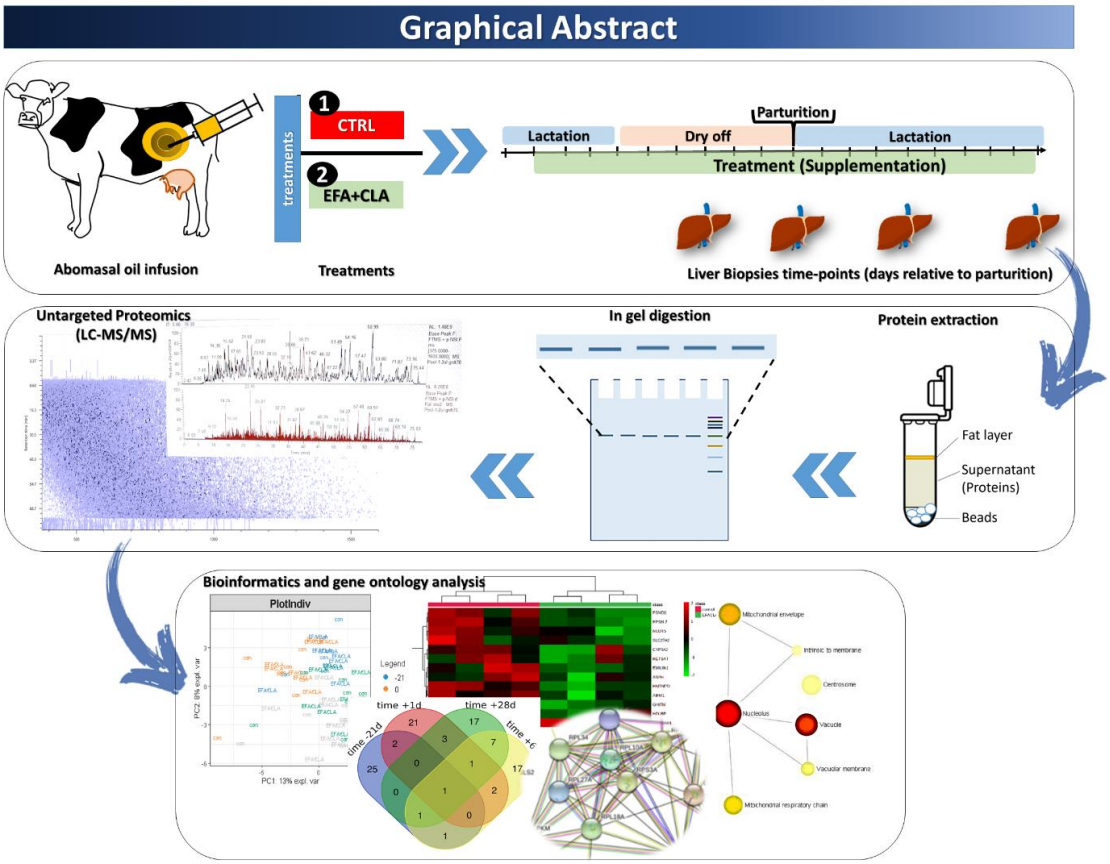

Abstract

This study aimed at investigating the synergistic effects of essential fatty acids (EFA) and conjugated linoleic acids (CLA) on the liver proteome profile of dairy cows during the transition to lactation. 16 Holstein cows were infused from 9 wk antepartum to 9 wk postpartum into the abomasum with either coconut oil (CTRL) or a mixture of EFA (linseed + safflower oil) and CLA (EFA+CLA). Label-free quantitative proteomics was performed in liver tissue biopsied at days -21, +1, +28, and +63 relative to calving. Differentially abundant proteins (DAP) between treatment groups were identified at the intersection between a multivariate and a univariate analysis. In total, 1680 proteins were identified at each time point, of which between groups DAP were assigned to the metabolism of xenobiotics by cytochrome P450, drug metabolism - cytochrome P450, steroid hormone biosynthesis, glycolysis/gluconeogenesis, and glutathione metabolism. Cytochrome P450, as a central hub, enriched with specific CYP enzymes comprising: CYP51A1 (d -21), CYP1A1 & CYP4F2 (d +28), and CYP4V2 (d +63). Collectively, supplementation of EFA+CLA in transition cows impacted hepatic lipid metabolism and enriched several common biological pathways at all time points that were mainly related to ω-oxidation of fatty acids through the Cytochrome p450 pathway.

Keywords: Liver Proteome, negative energy balance, postpartum, cytochrome p450, fatty acid oxidation, gene ontology

Significance

In three aspects this manuscript is notable. First, this is among the first longitudinal proteomics studies in nutrition of dairy cows. The selected time points are critical periods around parturition with profound endocrine and metabolic adaptations. Second, our findings provided novel information on key drivers of biologically relevant pathways suggested according to previously reported performance, zootechnical, and metabolism data (already published elsewhere). Third, our results revealed the role of cytochrome P450 that is hardly investigated, and of ω-oxidation pathways in the metabolism of fatty acids with the involvement of specific enzymes.

1. Introduction

Most mammals enter a state of negative energy balance (NEB) at the onset of lactation when the needs for lactation and maintenance cannot be met by feed intake. This metabolic status leads to mobilization of body reserves, mainly from adipose tissue in the form of non-esterified fatty acids (NEFA) to meet the energy requirements for lactation [1]. In high-yielding dairy cows, the liver plays a crucial role in metabolic homeostasis and energy production by metabolizing NEFA via precisely regulated signaling and cellular pathways [2]. However, hepatic lipid metabolism is impaired at the onset of lactation when uptake of NEFA by the liver exceeds their oxidation and the export capacity via lipoproteins and may thus result in a fatty liver syndrome [3].

Essential fatty acids (EFA), including linoleic acid (LA, 18:2 n-6) and α-linolenic acid (ALA, 18:3 n-3), affect the energy and FA metabolism, inflammation, and immune responses through activation of nuclear receptors [4-6]. Conjugated Linoleic Acids (CLA) which are stereo-isomers of LA have been reported to induce milk fat depression (MFD), thus partitioning energy by sparing milk energy for other organs [7, 8]. Energy spared from reduced milk fat synthesis was shown to affect energy partitioning, as toward adipose tissue fat stores [9, 10] and consequently to decrease plasma NEFA concentration and the risk for fatty liver [11]. The shift in dairy farming towards modern indoor production systems went along with a change from using pasture (grass) to feed rations that are largely based on so-called total mixed rations (TMR), in which the roughage component is mainly corn silage in many countries. The decreased or lacking consumption of fresh grass leads to a drop in the intake of ω-3 FA and CLA production [12-14]. A large body of work has highlighted the increased body deposition of n-3 FA and CLA in dairy cows fed with fresh grass in comparison to corn silage (for example [15]).

Assessing the effects of specific FA in different feeding practices is complex. Using an experimental model in which dairy cows receiving a corn-silage-based ration without any grass, the EFA and CLA's effects were tested by abomasal supplementation avoiding microbial degradation in the forestomaches [11, 16, 17]. The results showed that the FA marginally improved metabolic health by induction of MFD, which increased energy balance and reduced plasma concentration of triglycerides and NEFA. In addition, paraoxonase, a hepatic antioxidant enzyme, was elevated postpartum (PP) by the FA application. Although some of these impacted metabolites and proteins were directly or indirectly related to the liver, EFA and CLA-driven hepatic responses remain to be investigated.

Improvements in proteomics in the last decade have increased our understanding of the biological pathways impacted by various physiological conditions and diseases [18]. Characterization and comprehensive proteome profiling of the liver as a central organ in energy and lipid metabolism could open up new insights into the regulatory metabolic pathways influenced by different nutritional supplements. Proteomics results allow better understanding and predicting the metabolism and help define rapid biomarkers for use in the early diagnosis of steatosis or other metabolic diseases associated with liver metabolic health [19]. In this regard, there are several studies in dairy cows entailing the liver proteome for investigating feed efficiency [20], fatty liver [21], and heat stress [22, 23]. In the current study, untargeted proteomics was applied on liver samples from dairy cows supplemented or not with EFA and CLA to investigate metabolic responses during several critical time points around parturition. To the best of our knowledge, this is the first proteomics report considering the longitudinal response of EFA and CLA in dairy cows during the transition from late pregnancy to early lactation.

2. Material and methods

2.1. Animals, Treatments, and Experimental Design

The trial was carried out as described previously [11] with 16 multiparous (second lactation) German Holstein cows at the Research Institute for Farm Animal Biology (FBN), Dummerstorf, Germany. The experimental animal procedures were evaluated and approved by the German Animal Welfare Act (Landesamt für Landwirtschaft, Lebensmittelsicherheit und Fischerei Mecklenburg-Vorpommern, Germany; LALLF M-V/TSD/7221.3-1-038/15). More details on housing, feeding, feed intake, performance, and milk production of studied cows were presented earlier [11]. Briefly, dairy cows housed in a free-stall and abomasally injected with 1-control, the coconut oil (CTRL, n = 8; Bio-Kokosöl #665, Kräuterhaus Sanct Bernhard, KG, Bad Ditzenbach, Germany) or 2- EFA+CLA, a combination of linseed oil (DERBY® Leinöl #4026921003087, DERBY Spezialfutter GmbH, Münster, Germany), safflower oil (GEFRO Distelöl, GEFRO Reformversand Frommlet KG, Memmingen, Germany) and Lutalin® (CLA, n = 8; cis-9, trans-11, 10 g/d trans- 10, cis-12 CLA, BASF SE, Ludwigshafen, Germany) for 18 weeks started from d 63 antepartum (AP) until d 63 PP (Figure 1 A). Supplements were injected twice daily at 0700 and 1630 h in equal portions through abomasal infusion lines (Teflon tube [i. d. 6 mm] with 2 perforated Teflon flanges [o.d. 120 mm], placed in rumen cannulas (#2C or #1C 4'', Bar Diamond Inc., Parma, ID). The amount and FA composition of the lipid supplements is given in Supplementary, Table S1.

The cows were fed a conventional corn silage-based total mixed ration (TMR), formulated using the equation published by the German Society for Nutrition Physiology (2001 [24], 2008 [25], 2009 [26]) and Deutsche Landwirtschaftliche Gesellschaft (DLG, 2013) [27], for AP and PP. The basal diet was provided ad libitum at 0600 h, with free access to water and trace-mineralized salt blocks. The ingredients and chemical composition of the experimental diets are presented in Supplementary Table S2.

2.2. Liver biopsies

Liver tissue samples were obtained using a biopsy needle (outer diameter of 6 mm) under local anesthesia on d -21 AP, d 1 and d 28 PP, and after slaughtering the cows on d 63 PP as previously described [28] (Figure 1 A). The specimens were immediately frozen in liquid nitrogen and stored at −80 °C until protein extraction.

2.3. Liver Preparation for Proteomics Analysis

Frozen samples were first ground mechanically using a mortar and pestle chilled in liquid nitrogen. Eighty mg of tissue powder were placed in a reinforced 2-mL tube containing six ceramic beads (Dutscher, United Kingdom) and mixed with 1 mL of freshly prepared Laemmli sample buffer (50 mM Tris pH 6.8, 2% SDS, 5% glycerol, 2 mM DTT, 2.5 mM EDTA, 2.5 mM EGTA, H2O 920 µLl, 2x phosphatase inhibitors tablets (Perbio, Thermo Fischer, Hercules, California, USA), 1x protease inhibitor (Roche, Boulogne-Billancourt, France), 4 mM sodium orthovanadate, and 20 mM sodium fluoride). Subsequently, liver tissue was homogenized in a Precellys® 24 homogenizer (PEQLAB Biotechnology GmbH, Erlangen, Germany) at 6800 rpm, 3 x 30 sec (30-sec break between each cycle) at room temperature (RT). Immediately after the homogenization step, tubes were boiled for 10 min in 100 °C boiling water,

followed by centrifugation for 15 min at 16000 g at RT. The supernatant was carefully separated and stored at −80 °C until proteomics analysis. An aliquot of the lysate was used to measure the total protein concentration using the bicinchoninic acid (BCA, Pierce, Rockford, IL) assay. For peptide preparation, 100 µg of protein were first concentrated in 1D SDS-PAGE gel containing 5-15% acrylamide for stacking and resolving gel, respectively. Once the proteins enter the resolving gel, the electrophoresis was stopped and a small piece of gel containing a major band was cut. After reduction and alkylation, proteins were subjected to in-gel digestion with 10 ng/µL porcine trypsin (Promega, Madison, Wisconsin, United States) overnight (Figure 1 B).

2.4. Nano-LC-MS/MS Analysis

After digestion, the liver peptides mixture was analyzed using nano-scaled liquid chromatography (LC) in Ultimate 3000 RSLCnano system (Dionex) coupled to an Orbitrap Q Exactive HF-X mass spectrometer (Thermo Fisher Scientific) for mass spectrometry (MS), adopting the methods previously described by [29]. To reduce between-group variability, the LC-MS/MS was performed on all 64 samples consecutively and samples were randomly injected without any order related to time or treatment.

Briefly, a reversed-phase LC was carried out by loading 1 µL of the resuspended peptide mixture onto a trapping column (pre-column 5 mm length X 300 µm; Acclaim PepMap C18, 5 µm, 100 Å) equilibrated with trifluoroacetic acid 0.05% in water, at a flow rate of 30 µL/min. After 6 min, the pre-column was switched in-line with the analytical column (Acclaim PepMap 100 - 75 µm inner diameter × 25 cm length; C18 - 3 µm -100Å, Dionex), equilibrated with 96% solvent A (99.5% H_2O, 0.5% formic acid) and 4% solvent B (99.5% ACN, 0.5% formic acid).

Peptides were eluted at a 400 nL/min flow rate according to their hydrophobicity using a 4 to 20% gradient of solvent B for 60 min. Briefly, the analytical column was first equilibrated with 96% A solvent and 4% B solvent for 6 min, followed by a gradual increase of the B solvent to 20% for 70 min. Then, to clear the system from hydrophobic peptides, the B gradient rose from 20 to 80% in one min (at 77 min) and remained constant for further 5 minutes. Subsequently, the concentration of solvent B was decreased to 4% within 0.1 min and kept constant for 8 min to prepare the system for the next injection.

The nanoelectrospray ion source (Proxeon) was used as a connecter between the LC and Q Exactive HF-X mass spectrometer (Thermo Scientific). Eluates of LC step electro sprayed in positive-ion mode at 1.6 kV through a nanoelectrospray ion source heated to 250 °C. The Orbitrap Q Exactive HF-X MS used in HCD top 18 modes (i.e. 1 full scan MS and the 18 major peaks in the full scan selected for MS/MS). The mass spectrometry method duration was set to 79 min, the polarity was positive, and the default charge was 2.

On the MS1 scan, the parent ions were selected in the orbitrap Fourier transform mass spectrometry (FTMS) at the following parameters: a resolution of 60,000, an injection time of 50 ms. mass ranges from 375 to 1600 m/z and the Automatic gain control (AGC) target is set on 3 × 106 ions. Each MS analysis was followed by 18 data-dependent MS2 scans with an analysis of MSMS fragments at a resolution of 15,000, 1 × 105 AGC, and an injection time of 100 ms. The HCD collision energy set to 28% NCE, and ~15 s dynamic exclusion.

2.5. Processing of raw mass spectrometry data

The processing of raw Peptide MS/MS spectra was performed in Progenesis QI software (version 4.2, Nonlinear Dynamics, Newcastle upon Tyne, UK) using automatic alignment to the reference sample automatically defined by the software with the default parameter settings (maximum allowable ion charged set to 5 and Ions ANOVA p-value < 0.05). The mass generating function (mgf) list containing the detected and the quantified peptide ions were directly exported to MASCOT (version 2.5.1) interrogation engine and searched against a *Bos taurus* decoy database (Uniprot, download date: 2019/11/07, a total of 37,513 entries). The search criteria were set as follows: an enzyme digest of a protein set to trypsin, tryptic specificity required (cleavage C-terminal after lysine or arginine residues); 2 missed cleavages were allowed; carbamidomethylation (C) and oxidation (M) set as variable modification. The mass tolerance was set to 10 ppm for precursor ions, 0.02 Da for fragment ions, and FDR < 0.01. The identified peptides from the database search were imported back to Progenesis QI, and the corresponding proteins were identified and quantified based on the intensities of the specific validated peptides. Strict exclusion criteria (deamidated, carbamidomethyl, and oxidation contaminant proteins, having at least two peptides and two unique peptides, and presence in at least 50% of the samples in each treatment group/time point) were applied before analysis.

2.6. Data pre-processing

Statistical analyses were performed using the normalized intensity values combined with some in-house developed, EnhancedVolcano, MetaboAnalystR 3.0, and mixOmics R-packages in R statistical software (R version 4.0.0). Before the analyses, the following modifications were applied to proteins, in very severe filtrations: proteins with less than two unique peptides or having zero values in more than 50% of the replicates were not included in the analysis. After filtration, the log10 transformation and auto-scaling (z-transformation), which is mean-cantered and divided by the standard deviation of each variable applied to normalized intensities. The missing or zero values (indicated the peak did not reach the detectable thresholds) were imputed and replaced with the small values (half of the smallest positive value in the dataset). The PCA scatter plot was used to visualize the 2-D cross-section of hyperspace between samples and to distinguish the samples located far away from the treatment clusters (potential outliers). One cow (from the CTRL group in time point -21d AP) considered an outlier by both principal component analysis and hierarchical clustering was removed from the analysis

2.7. Statistical analyses

The selection of the most important proteins (VIP) involved in the discrimination of the CTRL and EFA+CLA groups at each time point was based on the intersection of two complementary analyses.

2.7.1 Multivariate analysis

Firstly, PCA analysis was done to reduce the dimension of data and to visualize clustering of samples regardless of treatment groups. Partial Least Square Discriminant Analysis (PLS-DA) analysis (mixOmics package in R) ranked proteins importance in projection scores of the first two components (PC1 and PC2) in each time point. This step aims to rank the most discriminative proteins that contribute to cluster separation between treatment groups. A permutation test (defined to 100 random computations) was applied to disprove the over-fitting of the PLS-DA model. Since the

permutation test indicated over-fitting in all time points, we performed the second filtration step according to univariate analysis. Although this study aimed to compare different treatments, not assessing populations parameter or identifying predictive model, therefore, permutation test's significance was not the case.

2.7.2 Univariate analysis

Secondly, from those proteins that were top VIP-ranked (score > 1.5), only ones with P-value < 0.05, and log2 (fold change) >1.3 (metaboanalyst R package) were considered as differentially abundant proteins (DAP) for further analysis. The P-value was assessed either by Student's t-test (parametric) or Wilcoxon Mann-Whitney test (non-parametric), according to the normality distribution of each protein (Shapiro-Wilk-Test) as previously described [30].

2.7.3 Intersection between multivariate and univariate analyses to identify discriminative and differentially abundant proteins (DAP)

The intersection between the results from the two methods was chosen to reduce the list of relevant proteins involved in the treatment effect. Thus, we considered two filters, and we selected the proteins that passed through both by choosing the intersection between the two complementary methods. Hierarchical clustering Heat map analysis was performed to approve and visualize DAP (Figure 1 C).

2.8. Bioinformatics analysis of differentially abundant proteins

Before bioinformatics analysis, proteins' accession was converted into Gene ID using the UniProt (retrieve/ID mapping) database conversion tool, and undefined proteins were blasted and replaced with their Gene ID in *Bos taurus* and *Homo sapiens*. Then, the gene ontology (GO) analysis containing Biological Process (BP), Molecular Function (MF), and Cellular Component (CC), Kyoto Encyclopedia of Genes and Genomes (KEGG), and Reactome pathways enrichment analysis of the DAP were performed in STRING web tool version 11.0 in Cytoscape and ProteINSIDE (version 1.0) constructed specifically under *B. taurus* interactions map. Only pathways with adjusted P-value < 0.05 (corrected to false discovery rate with Benjamini-Hochberg method) and having at least two hits in each pathway were considered as significantly enriched (Figure 1 C). REVIGO web server (http://revigo.irb.hr/) was used to summarize BP terms. Generated GO terms were submitted to Cytoscape version 3.8.2 and Networkanalyst.ca version 3.0 to build the interaction networks. Protein protein interaction networks was constructed by inputting the DAP in each time point to STRING and visualized in cytoscape software, in which nodes and edges represent proteins and their interactions, respectively [31].

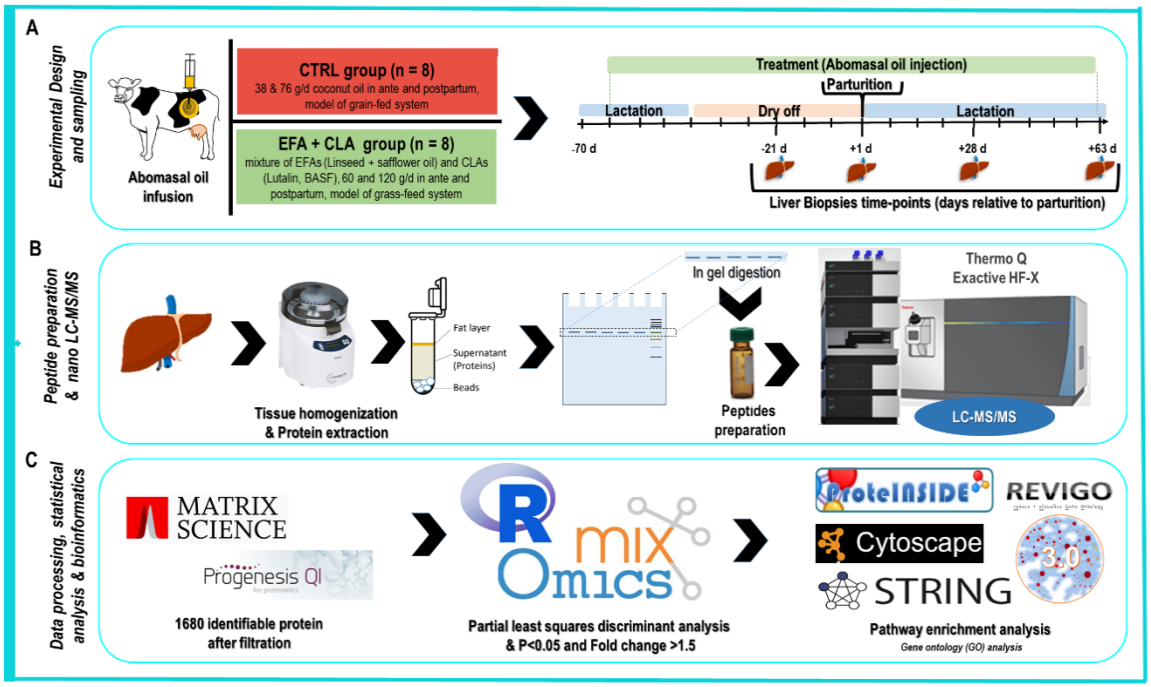

Figure 1) Schematic diagram of the (A) study design, (B) proteomics workflow, and (C) bioinformatics pipeline. (A) Timeline of treatments supplementation (from -63d ante to +63d postpartum) and liver biopsy collection (-21 d, +1 d, +28 d, and +63 d relative to parturition). Bold lines indicate liver biopsy sampling timepoints. (B) Protein extraction, purification, reduction, alkylation, and digestion; peptides were analysed by high-resolution LC-MS/MS, (C) Peptides alignment (progenesis), and protein identification (mascot) procedure were performed by Progenesis software coupled with the Mascot search engine, statistical analysis was based on Partial least squares discriminant analysis (PLS-DA) merged with $P < 0.05$ and Fold change > 1.5, followed by bioinformatics analysis (protein-protein interaction and Gene Ontology (GO) enrichment analysis.

3. Results

3.1. Cows performance data

A summary of cows performance and plasma metabolites data from the CTRL and EFA+CLA group was extracted from [11, 16, 17] and provided in supplementary S3 and S4. In brief, EFA+CLA supplementation increased plasma concentration of these FA, decreased PP NEFA and TG content, induced MFD, increased energy balance, and slightly affected markers of ketogenesis and hepatic inflammation (i.e., haptoglobin and paraoxonase). Dry matter intake, body weight, milk yield, and net energy intake were not affected by treatment.

3.2. Liver proteome profile

Out of 2720 identified proteins, a total of 1680 proteins at each time point were maintained for statistical analysis after applying the exclusion criteria [31]. Of the 1680 proteins,1614 proteins were annotated by GO terms related to 907 BP, as well as 111 KEGG, and 270 Reactome pathways that covered a diverse range of metabolic pathways related to metabolism (carbohydrate, energy, lipid, nucleotide, amino acid, glycan, vitamin, and xenobiotic metabolism), genetic

information processing (translation and folding, sorting and degradation), cellular process (transport and catabolism and cell growth and death), and organismal systems (immune system and endocrine system).

3.3. Differentially abundant proteins and functional enrichment at day 21 antepartum (Figure 2 A),

From the total identified proteins, 29 proteins were differentially abundant on 21 d AP (Table 1), in which the relative abundance of 19 proteins was increased with a fold change that ranged from 1.43 - 3.92 (P-value < 0.05), and ten proteins were decreased (ranging from 0.38 - 0.70 fold, P-value < 0.05) in the EFA+CLA group when compared to the CTRL group. The DAP were further approved by clustered Heat map and are presented in Figure 2 (A, B, and C). The overabundant proteins were annotated by GO terms related to “cholesterol biosynthetic process (GO:0006695)” and “lipid metabolic process (GO:0006629)” (Figure 2 D, details in [31]). Underabundant proteins were not annotated by any GO terms.

Considering all DAP, “steroid biosynthesis (bta00100)”, “metabolism of xenobiotics by cytochrome P450 (bta00980)”, “drug metabolism - cytochrome P450 (bta00982)”, “retinol metabolism (bta00830)”, “metabolic pathways (bta01100)” were mapped to KEGG metabolic pathways (Figure 2 E, details in [31]).

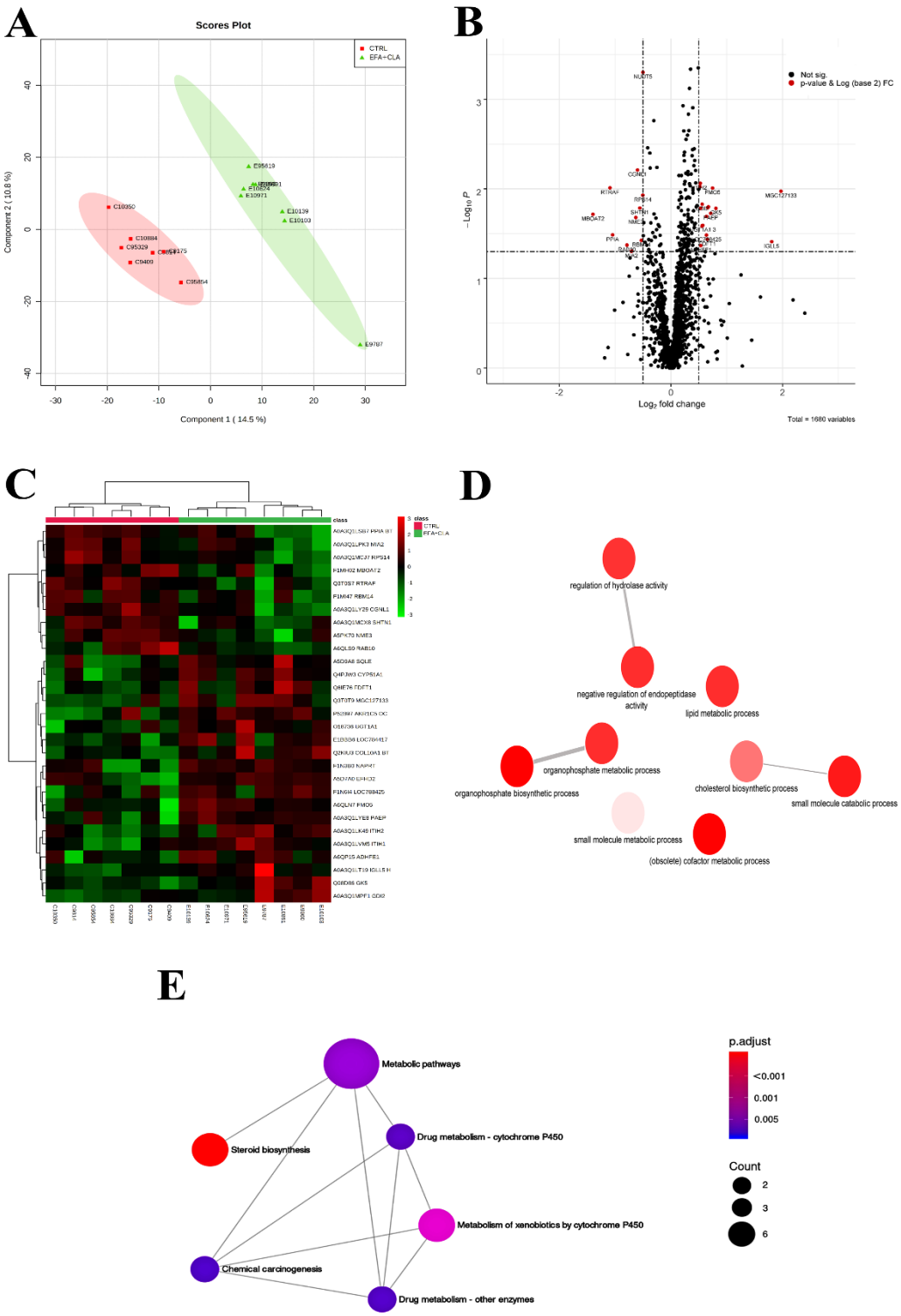

Figure 2) A. Partial least squares discriminant analysis (PLS-DA) score plot of CTRL (red squares) and EFA+CLA (green triangle) on day 21 antepartum. B. Volcano plot represents differentially abundant proteins between CTRL and EFA+CLA group, increased (top right) and decreased (top left) proteins were highlighted in red (P<0.05 and fold change>than 0.58 in a log scale that means a fold change of 1.3). C. Hierarchical clustering heat map analysis of differentially abundant proteins; Rows and columns are sorted by similarity as indicated by the left (proteins) and top (samples) dendrograms, red and green represent CTRL and EFA+CLA, respectively. D. Biological Process Ontology for the differentially

abundant proteins (DAP). Fold enrichment (Bars, –log10 (adjusted P-value)) refers to the number of relevant gene names represented in each category relative to random expression of all genes in the *Bos taurus* genome. The line between pathways represents their dependence. E. KEGG pathways map of DAP. The colour of the nodes represents the –log10 (adjusted P-value); the size of the dots represents the number of DAP in the pathway. The line between pathways represents their dependence.

3.4. Differentially abundant proteins, interaction network, and functional enrichment of day 1 postpartum,

On the day after parturition, 12 proteins were differentially abundant between treatment groups (Table 1), including nine increased proteins (with a fold change that ranged from 1.50 - 4.16, P-value < 0.05), and three decreased proteins (ranging from 0.37 - 0.67) in the EFA+CLA group. The DAP are shown in a Volcano plot, and their expression was plotted by heat maps (Figure 3 A, B, C).

Also, the DAP were annotated by KEGG pathways, including “drug metabolism - cytochrome P450 (bta00982)” and “metabolism of xenobiotics by cytochrome P450 (bta00980)” (Figure 3 D) and Reactome pathway “metabolism of lipids (bta556833)” (Figure 3 E, details in [31]).

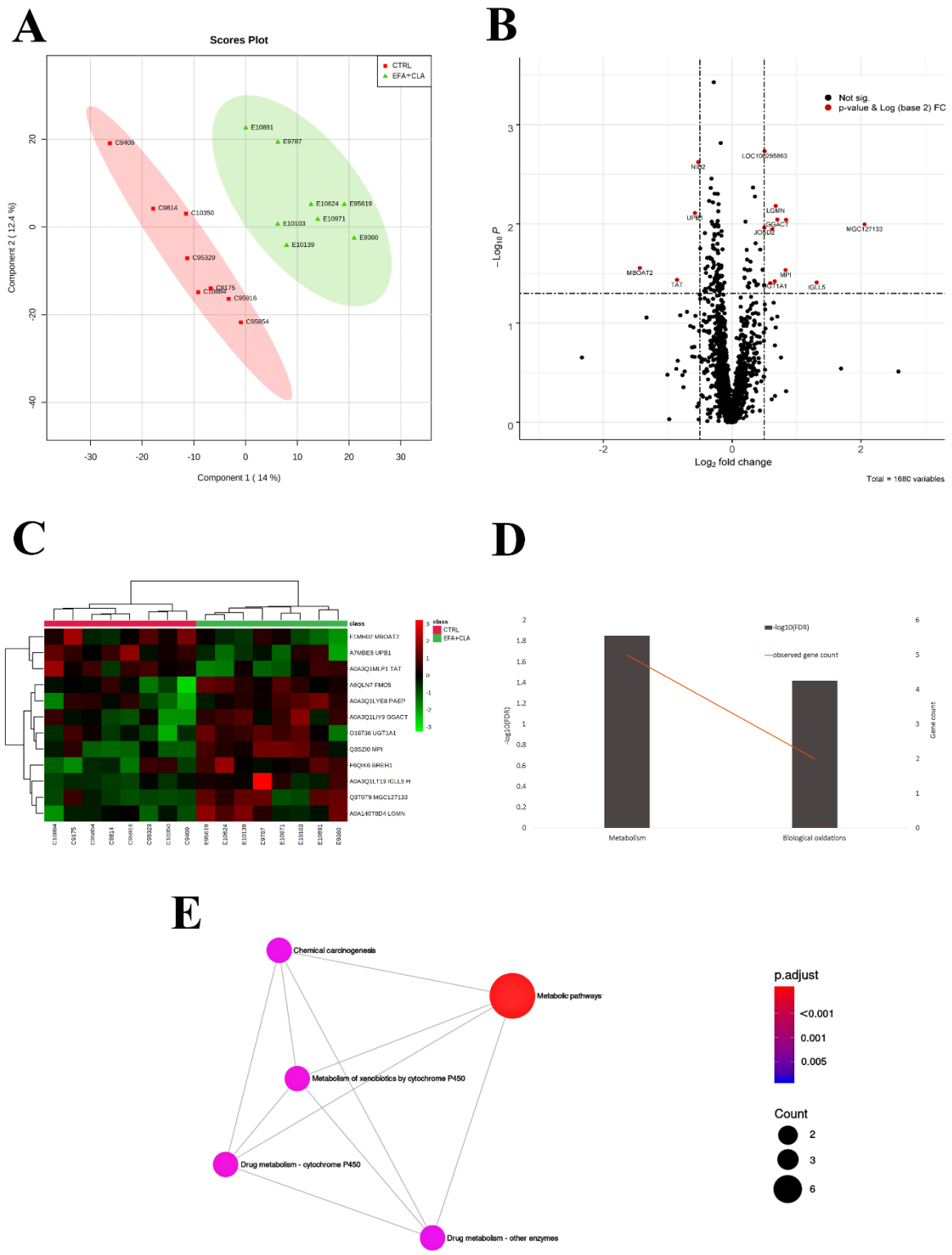

Figure 3) A. Partial least squares discriminant analysis (PLS-DA) score plot of CTRL (red squares) and EFA+CLA (green triangle) in day 1 of postpartum. B. Volcano plot represents differentially abundant proteins between CTRL and EFA+CLA group, increased (top right) and decreased (top left) proteins were highlighted in red (P<0.05 and fold change>1.5). C. Hierarchical clustering heat map analysis of differentially abundant proteins, Rows and columns are respectively sorted by similarity as indicated by the left (proteins) and top (samples) dendrograms, red and green represent CTRL and EFA+CLA, respectively. D. Reactome enrichment analysis (x-axis), fold enrichment (bars, left y-axis); the number of

significant genes in each pathway (–log10, adjusted P-value) is represented by the lines on the right y-axis) represent. E. KEGG pathways map of differentially abundant proteins (DAP). The colour of the nodes represents the –log10 (adjusted P-value); the size of the dots represents the number of DAP in the pathway. The line between pathways represents their dependence.

3.5. Differentially abundant proteins, interaction network, and functional enrichment at day 28 postpartum,

At this time point, the relative abundance of 27 proteins was different between treatments (Table 1), of which 21 proteins were increased (with a fold change that ranged from 1.50 - 4.70, P-value < 0.05) and 6 proteins decreased (ranging from 0.57 - 0.66) in the EFA+CLA group as compared to the control group (Figure 4 A, B, C). Twenty-three BP have annotated (adjusted P-value < 0.05) by increased proteins, of which "cellular iron ion homeostasis (GO:0006879)", "apoptotic mitochondrial changes (GO:0008637)", "mitochondrial transport (GO:0006839)", "regulation of lipid metabolic process (GO:0019216)", "membrane organization (GO:0061024)", "apoptotic process (GO:0006915)", and "regulation of cellular process (GO:0050794)" (Figure 4 D, details in [31]). Moreover, the GO term "ferric iron-binding (GO:0008199)" in the MF category has been annotated. The proteins were localized in the "mitochondrial intermembrane space (GO:0005758)", "lysosome (GO:0005764)", and "cytoplasm (GO:0005737)", respectively ([31]).

Also, the KEGG pathways were linked to "ferroptosis (bta04216)", "mineral absorption (bta04978)", "porphyrin and chlorophyll metabolism (bta00860)", "drug metabolism - cytochrome P450 (bta00982)", "metabolism of xenobiotics by cytochrome P450 (bta00980)", "chemical carcinogenesis (bta05204)", "arachidonic acid metabolism (bta00590)", and "metabolic pathways (bta01100)" (Figure 4 E).

Decreased proteins were annotated by KEGG pathways related to "steroid hormone biosynthesis (bta00140)", "metabolism of xenobiotics by cytochrome P450 (bta00980)", and "chemical carcinogenesis (bta05204)" ([31]). Reactome enriched pathways included "arachidonic acid metabolism BTA-2142753", "cytochrome P450 - arranged by substrate type BTA-211897" and "metabolism of lipids BTA-556833" (Figure 4 F).

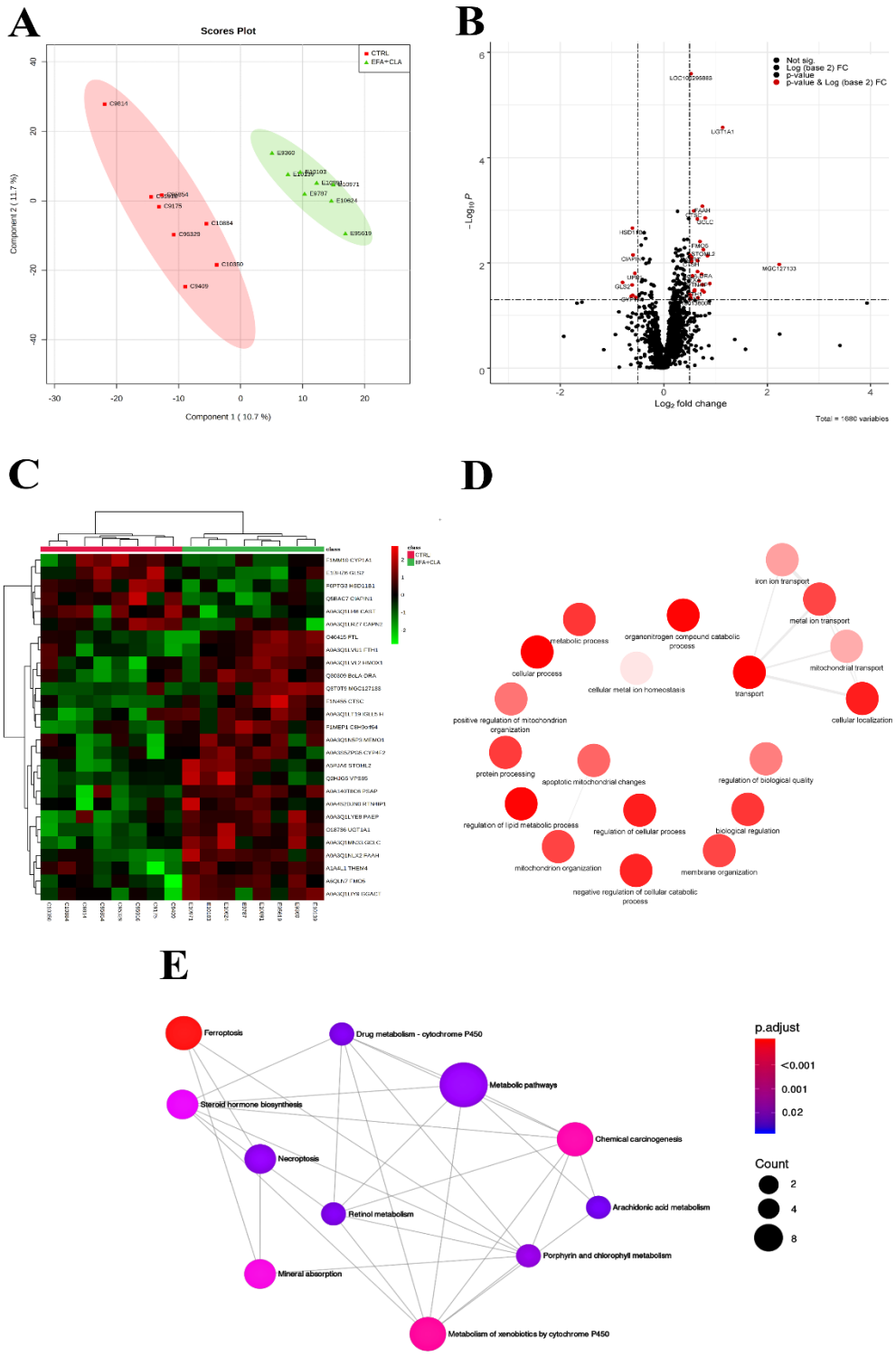

Figure 4) A. Partial least squares discriminant analysis (PLS-DA) score plot of CTRL (red squares) and EFA+CLA (green triangle) in day 28 of postpartum. B. Volcano plot represents differentially abundant proteins between CTRL and EFA+CLA group, increased (top right) and decreased (top left) proteins were highlighted in red (P<0.05 and fold change>1.5). C. Hierarchical clustering heat map analysis of differentially abundant proteins, Rows and columns are respectively sorted by similarity as indicated by the left (proteins) and top (samples) dendrograms, red and green represent CTRL and EFA+CLA, respectively. D. Biological Process Ontology for the differentially abundant proteins (DAP). The fold enrichment

(adjusted P-value) is coloured in red according to the degree of significance, refers to the number of relevant gene names represented in each category relative to random expression of all genes in the Bos taurus genome. The line between pathways represents their dependence. E. KEGG pathways map of DAP. The colour of the nodes represents the –log10 (adjusted P-value); the size of the dots represents the number of DAP in the pathway. The line between pathways represents their dependence.

3.6. Differentially abundant proteins, interaction network, and functional enrichment at day 63 postpartum,

At the last time-point, 26 proteins were considered as DAP (Table 1), among which 16 proteins were upregulated (with a fold change ranging from 1.49 - 4.16, P-value < 0.05), and 10 proteins were downregulated (ranged from 0.11-0.67) in the treatment group as compared to the CTRL group (Figure 5 A, B, C).

The decreased proteins annotated by KEGG pathways belong to “drug metabolism - cytochrome P450 (bta00982)”, “metabolism of xenobiotics by cytochrome P450 (bta00980)”, “chemical carcinogenesis (bta05204)”, and “metabolic pathways (bta01100)” (Figure 5 D, details in [31]). Interestingly, the same pathways were also enriched by the upregulated proteins (details in [31]). Moreover, DAP were annotated by Reactome terms to “metabolism BTA-1430728”, “Phase II - conjugation of compounds BTA-156580”, “glutathione conjugation BTA-156590” (Figure 5 E).

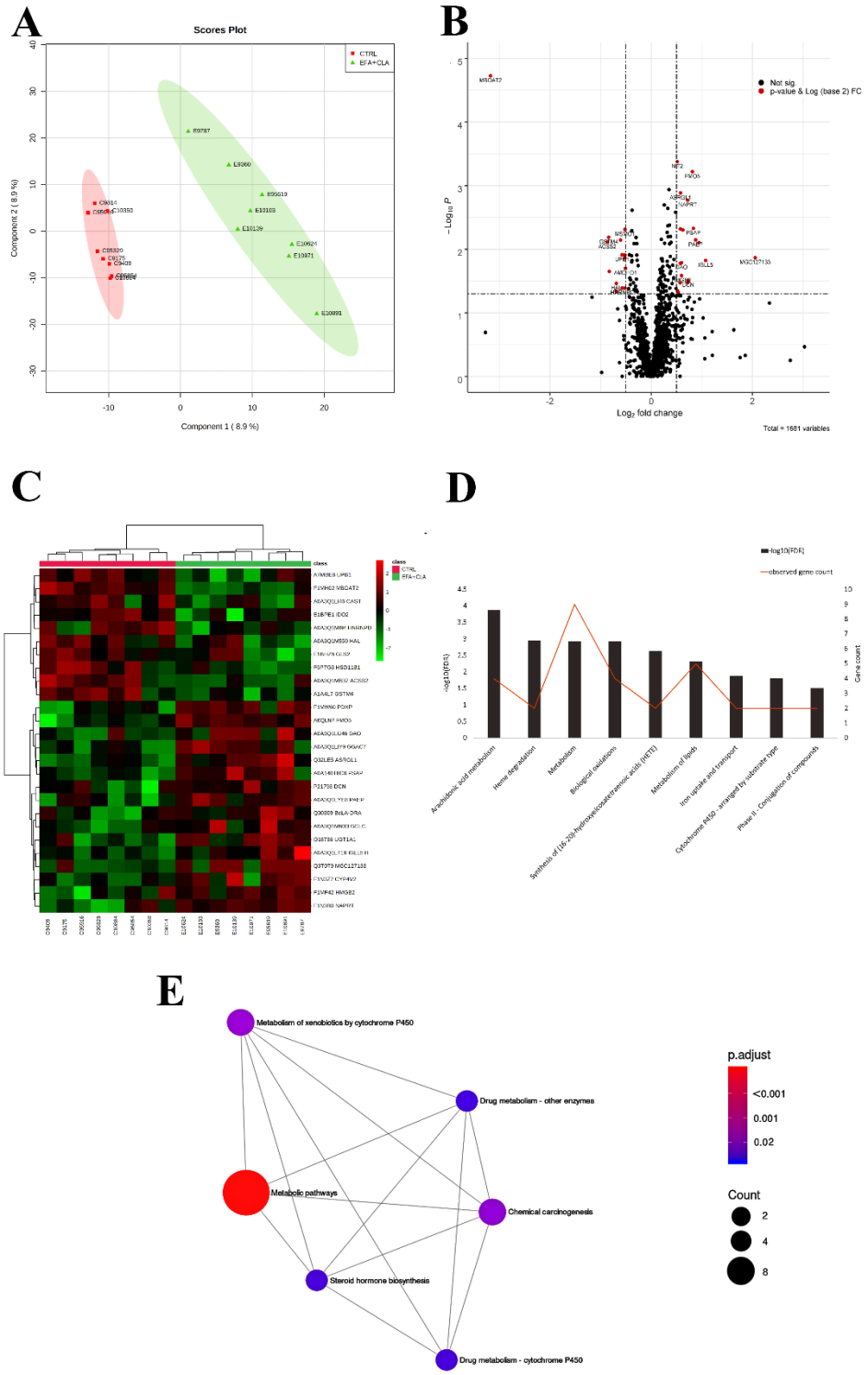

Figure 5) A. Partial least squares discriminant analysis (PLS-DA) score plot of CTRL (red squares) and EFA+CLA (green triangle) in day 63 of postpartum. B. Volcano plot represents differentially abundant proteins between CTRL and EFA+CLA group, increased (top right) and decreased (top left) proteins were highlighted in red (P<0.05 and fold change>1.5). C. Hierarchical clustering heat map analysis of differentially abundant proteins, Rows and columns are respectively sorted by similarity as indicated by the left (proteins) and top (samples) dendrograms, red and green represent CTRL and EFA+CLA, respectively. D. Reactome enrichment analysis (x-axis), fold enrichment (bars, left y-axis); the number of

significant genes in each pathway (–log10, adjusted P-value) is represented by the lines on the right y-axis) represent. E. KEGG pathways map of differentially abundant proteins (DAP). The colour of the nodes represents the –log10 (adjusted P-value); the size of the dots represents the number of DAP in the pathway. The line between pathways represents their dependence.

3.7. Common differentially abundant proteins along time

As illustrated in the Venn diagram (Figure 6), the DAP pattern was time-specific, probably due to substrates (i.e. supplemented FA, NEFA, and accumulated intermediates) abundance. The relative abundance of 5 common proteins including 20-beta-hydroxysteroid dehydrogenase-like (Q3T0T9, GN: MGC127133), lipocln_cytosolic_FA-bd_dom domain-containing protein (A0A3Q1LYE8, GN: PAEP), Ig-like domain-containing protein (A0A3Q1LT19, GN: IGLL5), dimethylaniline monooxygenase [N-oxide-forming] (A6QLN7, GN: FMO5), and UDP-glucuronosyltransferase (O18736, GN: UGT1A1) were affected by EFA+CLA treatment during all time points (Figure 5). Moreover, seven common proteins including glutamate-cysteine ligase catalytic subunit (A0A3Q1MN33, GN: GCLC), glutaminase 2 (E1BHZ6, GN: GLS2), calpain-2 catalytic (A0A3Q1LRZ7, GN: CAPN2)**,** calpastatin (A0A3Q1LI46, GN: CAST), boLA-DR-alpha (Q30309, GN: BoLA-DRA), prosaposin (A0A140T8C6, GN: PSAP), and hydroxysteroid 11-beta dehydrogenase 1 (F6PTG3, GN: HSD11B1) were affected by EFA+CLA treatment on days 28 and 63.

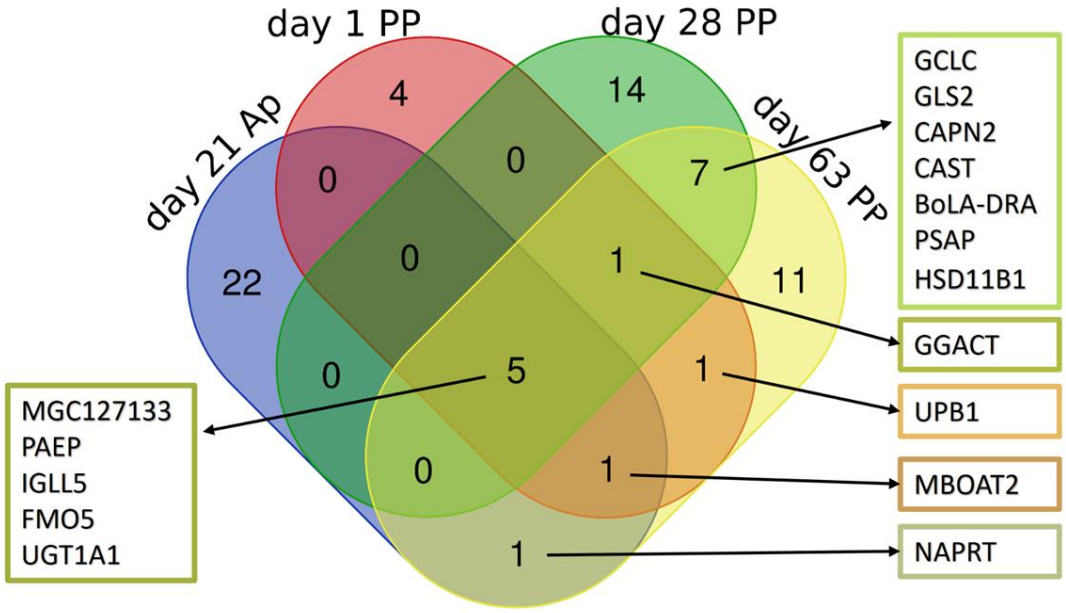

Figure 6) Venn diagram represent common and specific differentially abundant proteins identified in -21, +1, +28, and +63 days relative to parturition.

4. Discussion

This study aimed to investigate the metabolic adaptation in dairy cows supplemented with a combination of EFA and CLA during the transition from pregnancy to lactation by applying proteomics in liver tissue samples. The synergistic effect of these two FA on performances and "classical" parameters including energy metabolism, the somatotropic axis signaling pathway, plasma fatty acids profile, and markers of inflammation was recently presented [11, 16, 17]. The present study complements previously published works on the hepatic metabolic adaptations as it pointed out proteins and pathways that are part of the molecular signatures elicited by supplementation with EFA and CLA, the latter representing a model for feeding on grass.

4.1. Common pathways identified antepartum and postpartum

The relative abundance of MGC127133, PAEP, IGLL5, FMO5, and UGT1A1 was affected by EFA+CLA regardless of time (Figure 6). These proteins were annotated by KEGG pathways related to drug metabolism - cytochrome P450, metabolism of xenobiotics by cytochrome P450, and retinol metabolism, all belonging to the lesser-studied "cytochrome P450 epoxidation/hydroxylation" pathways involved in ω-oxidation of FA. Unfortunately, less information is available regarding these enzymes' specific functions or their associated pathways in dairy cows, especially in *in vivo* models. Nevertheless, in many species, particularly humans and mice, cytochrome P450 and xenobiotic metabolism regulate the cross-talk between the immune system and metabolism [32].

Cytochrome (CYP) refers to a superfamily of heme-containing membrane-associated enzymes, regulating several functions related to cholesterol and FA metabolism, detoxification of xenobiotic substances, steroid metabolism, drug and pro-carcinogen deactivation, and catabolism of exogenous compounds, located primarily in the liver, but also in all other tissues [33]. In this context, along with the α- and β-oxidation of FA, hepatic ω-oxidation of FA (CYP P450) can help utilize PUFA and prevent hepatic lipid overload [34]. ω-oxidation of FA is an alternative pathway when mitochondrial β-oxidation is deficient and involves the oxidation of the ω-carbon of FA in the endoplasmic reticulum to provide succinyl-CoA [35]. CYP isoforms may have different functions, activities, and substrates [36]; therefore, their inhibition and induction are regulated indirectly by ligand activation of xenobiotics to nuclear receptors, such as peroxisome proliferator-activated receptors (PPARs) [37] and pregnane X receptor (PXR) [38]. In this respect, xenobiotics are defined as natural components such as diet-derived compounds (e.g., lipids) or synthetic drugs considered foreign to the body and therefore being subjected to the liver metabolism primarily to increase their polarity and make them easier to excrete [39].

Previously, in a precise activity-based protein profiling technique, it has been shown that a commercial high-fat diet (based on lard) decreased P450 activity in mouse liver, which led to obesity, obesity-induced chronic inflammation, increased risk for hepatotoxicity, and metabolic disease [40]. Herein, we suppose that EFA and CLA or their intermediates acted as xenobiotic substances and oxidized through cytochrome P450 pathways. It is worth pointing out that any alteration to the average physiological level of CYP activities may cause disease, being their activity required to detoxify drugs, neutral components, or biochemical intermediates to avoid impeding critical metabolic pathways. Taken together, the low level of PUFA or n-3 to n-6 ratio in the CTRL group may negatively influence the

functional capacity of xenobiotic-metabolizing P450. Herein, the results indicated specific and different isoforms (isoform-specific manner) of CYP affected by treatment during the transition period.

Recent studies using knockout *Fmo5*$^{-/-}$ mice revealed that FMO5 not only functions as a xenobiotic-metabolizing enzyme but also has been implicated as a regulator of glucose and lipid homeostasis, metabolic ageing, and insulin sensitivity [41, 42]. In addition, FMO5 acts as NADPH oxidase, lowering NADPH which is the electron source in lipid and cholesterol biosynthesis. In this regard, downregulation of FMO5 in mice has been associated with reduced fat deposition and lower plasma cholesterol [41, 42]. Thus, the increased expression of this protein is probably induced by a xenobiotic-like function of supplemented FA.

4.2. Metabolic adaptation in the antepartum period

On d 21 AP, 4 proteins were annotated by enriched GO term related to cholesterol metabolism. In addition to FMO5 which is a DAP identified at all time points, squalene monooxygenase (A5D9A8, GN: SQLE, unreviewed proteins in *Bos taurus*) and squalene synthase (Q6IE76, GN: FDFT1, unreviewed proteins in *Bos taurus*) and CYP51A1 were increased in the EFA+CLA group. Previously in a human study, a significant association of CYP51A1 gene expression with lower blood total cholesterol and LDL cholesterol levels, but not with TG and HDL-cholesterol, has been reported in women in their second trimester of pregnancy [43]. The CYP51 protein is very conserved between species (NCBI homology, https://www.ncbi.nlm.nih.gov/); therefore, the same function of this protein in dairy cows can be supposed. However, in this study, total cholesterol and LDL cholesterol concentrations were not affected by treatment in the AP period (Figure S4).

Moreover, SQLE, FDFT1, and CYP51A1 are all involved in the cholesterol biosynthesis pathways through the Sterol regulatory element-binding proteins (SREBP)-activated mevalonate pathway [44, 45]. In this pathway, FDFT1 initiates the conversion of farnesyl-pyrophosphate to squalene, which is the first stage of liver cholesterol synthesis [46], followed by the synthesis of lanosterol from squalene catalyzed by SQLE, and the final step is the conversion of lanosterol to cholesterol by the action of CYP51A [47]. Cholesterol homeostasis is crucial for normal cellular and physiological functions and is strictly controlled by nuclear receptors, mammalian target of rapamycin (mTOR)/SREBP2 pathway [48] and Liver X Receptors (LXR) [49] which induce and inhibit its synthesis, respectively. In dairy cows, insufficiency of cholesterol metabolism and acceleration of body fat degradation before parturition was reported to be associated with developing ketosis PP [50]. On the other side, chronic hepatic expression of SREBP2 and excessive cholesterol storage has been shown to cause fatty liver disease (steatosis), hypertriglyceridemia, and insulin resistance in non-ruminant species [51]. Fortunately, no differences were observed in the plasma concentration of total cholesterol, TG, LDL, HDL (Figure S4), and hepatic expression of HMGCS2 between treatment groups before parturition [11, 17], which possibly points towards the feedback regulation that synthesized cholesterol was used to maintain its homeostasis crucial in pregnant cows. Indeed, as a structural component of the cellular membrane and precursor for steroid hormones, cholesterol esters, and bile acids (BA), cholesterol is essential for the normal development of the dam and the fetus. In humans and rodents with a hemochorial or hemoendothelial placenta type, the fetus depends on exogenous cholesterol sources obtained from the maternal circulation transported across the placenta, mainly through lipoproteins [52]. It is not known whether this applies for

species with an epitheliochorial placenta type, such as most farm animals. Also, BA are incorporated into lipoproteins and may induce hepatocytes to secrete and export the accumulated lipids from the liver (for review [53]). Intrahepatic cholestasis and elevated BA and/or transaminases are considered as a liver disease [54].

Moreover, antepartum and around parturition, the membrane-bound O-acyltransferase 2 (F1MH02, GN: MBOAT2, also known as lysophosphatidylcholine acyltransferase 4), a newly discovered member of the MBOAT family [55] was decreased in the EFA+CLA group. This conserved enzyme catalyzes the production of glycerophospholipids in the mammalian cell membrane, particularly phosphatidylcholine and phosphatidylethanolamine, which determine membrane intrinsic curvature and fluidity [56]. This is the first study reporting the expression of MBOAT2 in dairy cows' hepatocytes, and it is probably involved in modulating the ratio of PUFA in cellular membranes.

4.3. Metabolic adaptation in lactation

The day after parturition, along with cytochrome P450 pathways, the catabolic process and proteolysis, and bile secretion KEGG pathways were annotated by DAP in the EFA+CLA group (identified by PLS-DA analysis). The upregulated solute carrier organic anion transporter family member 1B3 (F1MYV0, GN: SLCO1B3) enzyme not only incorporates with activation of BA secretion [57] but also in the uptake of endogenous and xenobiotic compounds [58]. Apart from already discussed mechanisms, BA has been reported to play novel roles as signaling molecules regulating energy homeostasis, TG concentrations, and glucose [59-61]. In this regard, in a transcriptomic study, the BA synthesis pathway reduction was reported in dairy cows with severe compared to mild negative energy balance[62].

The liver is the main site regulating BA synthesis [40], primarily through the cholesterol/lipid homeostasis pathway [63]. The activated mevalonate pathway thereby increased cholesterol synthesis that was discussed for the last time-point, probably induced the downstream pathway, BA synthesis, and may explain why cholesterol concentration was not different between treatments. More interestingly, converting cholesterol to BA, is regulated by cytochrome P450 (CYP7a1 and CYP8b1) pathways [40], although neither CYP7a1 abundance nor CYP8b1 were affected by treatment. This may propose other pathways besides cytochrome P450 to regulate this conversion in dairy cows. Nevertheless, no remarkable differences in performance and metabolite were observed between treatments. The difference in energy balance between treatment groups [11] may indicate that the more negative energy balance in the CTRL group had impaired cholesterol and BA synthesis.

On day 28 PP, cytochrome P450 family 4 subfamily F member 2 (A0A3S5ZPG5, GN: CYP4F2) and cytochrome P450 family 1 subfamily A member 1 (F1MM10, GN: CYP1A1) had higher and lower abundance in the EFA+CLA group, respectively. In this regard, a study in mice reported decreased CYP4F2 protein in the liver upon feeding a high-fat diet associated with impaired hepatic lipid metabolism α-tocopherol pathways [64]. In general, the CYP4 members are tissue-specific and involved in FA metabolism, maintaining the concentration of FA and FA-derived bioactive molecules within a normal physiological range [65]. CYP4F2 [66] and CYP4V2 [67] are two important members of this family and are highly abundant in the liver. Arachidonic acid, lauric acid, vitamin K, and leukotriene are the specific substrates for the CYP4F2 enzyme [68, 69]. We observed a significant difference in the plasma concentration of FA on day 28 PP with lesser values in the EFA+CLA group. The greater FA concentration in the

CTRL group may have impaired mitochondrial function, reduced ATP synthesis, and potentially triggered lipotoxicity [70]. On the other hand, an overabundance of CYP4F2 in the EFA+CLA group has been reported in humans to amplify the capacity of hepatocytes to oxidize excess FA [71], which may support our proteomic results. Induction of CYP4F2 expression is proposed to be mediated by the ligand activation of nuclear receptors with supplemented FA and in response to activated AMPK and SREBP pathways, which then augment the capacity of cytochrome P450 to oxidize xenobiotics [71]. However, regulation may be at the level of enzyme activity rather than of protein abundance, since enrichment of these two pathways was not observed in the present study. In other words, during the negative energy balance, when the liver is stressed by the excessive FA supply from lipogenesis that may cause lipotoxicity, the activation of CYP4F2, which removes FA, is logic and may explain how the EFA+CLA group accomplish the inhibition of steatosis.

On the other side, the members of the CYP1 family use endogenous sex hormones such as progesterone and testosterone, amine hormones like melatonin, vitamins, FA such as linoleic acid, and phospholipids as substrates [72], which under specific circumstances activate compounds that react with DNA leading to an imitation of the mutagenic process [73]. Furthermore, it has been reported both in *in vivo* [74] and *in vitro* [75-77] studies that CYP1A1 is involved in PUFA metabolism.

Previously, the xenobiotic-like potential of fish oil in the induction of CYP1A1 mRNA expression in primary cultured bovine hepatocytes was reported [78]. Also, there is emerging evidence that induction of CYP1A1 leads to non-alcoholic fatty liver disease and the development of oxidative stress in humans, which is another molecular support for hepatic metabolic imbalance in our CTRL group [79]. The exact mechanism of how CYP1A1 was inhibited in EFA+CLA is not yet precisely known, although based on a study in mice [80], it could be speculated that transcriptional regulation of CYP450 through activation of PPARα is likely a possible pathway.

During the PP period (d +28 and +63), 11β-hydroxysteroid dehydrogenase type 1 (F6PTG3, GN: HSD11B1) and glutamate-cysteine ligase catalytic subunit (A0A3Q1MN33, GN: GCLC) increased, and phosphate-activated mitochondrial glutaminase (E1BHZ6, GN: GLS2) decreased in EFA+CLA (Figure 5). Among them, GCLC and GLS2 are involved in the glutamine and glutamate metabolic processes and the glutathione (GSH) system. In GSH biosynthesis, GLS2 catalyzes the conversion of glutamine to glutamate [81], and GCLC is a rate-limiting enzyme in converting glutamate to GSH [82]. The combination of the above-noted enzymatic changes would be expected to result in glutamate regulation. Glutamate, as one of the most abundant amino acids in the liver, is considered to be at the crossroads of hepatic metabolism, where it is mainly involved in the TCA cycle, gluconeogenesis, FA oxidation [83], and electron transport from the cytoplasm into the mitochondria via the malate-aspartate shuttle [84].

The HSD11B1 is an endoplasmic reticulum-located reductase that activates cortisone to cortisol, thereby modulating hepatic gluconeogenesis [85]. It also plays a crucial role in glucocorticoid receptor (GR) activation, which in turn is involved in the regulation of anti-stress and anti-inflammatory pathways [86]. It has been previously shown that liver synthetized BA inhibit the HSD11B1 [87], which may be related to the downregulation of HSD11B1.

On day 63 PP, cytochrome P450 family 4 subfamily V member 2 (F1N3Z7, GN: CYP4V2) was more abundant in the EFA+CLA than in the CTRL group. CYP4V2 has the same characteristic as the CYP4 classes but preferably metabolizes arachidonic acid, lauric acid, eicosapentaenoic acid, docosahexaenoic acid, and medium-chain FA as

substrates [67, 88, 89]. The greater abundance of different CYP isomers between d 28 and 63 PP, probably related to FA concentration, may compete with EFA and CLA for ligand activation of nuclear receptors (substrate dependent). At this time point that coincides with returning to positive EB, the previously enriched cytochrome P450 pathways and steroid hormone biosynthesis were affected by both downregulations of HSD11B1, glutathione S-transferase Mu 4 (A1A4L7, GN: GSTM4), and upregulation of MGC127133 and UGT1A1. Moreover, enrichment of several KEGG pathways in the EFA+CLA group was observed by PLS-DA-identified DAP related to pentose and glucuronate interconversions, starch and sucrose metabolism, pyruvate metabolism, glutamate metabolic process, and glycolysis/gluconeogenesis. These pathways are intimately interconnected and are associated with energy metabolism. Therefore, we considered these alterations to restore metabolic adaptation to the normal metabolism in positive EB status. The EFA+CLA cows turned back to a positive EB around 21 days earlier than the CTRL group [11]. Therefore, the activated metabolic adaptive processes in response to the NEB were also switched off or returned to normal functions faster.

5. Conclusion

The results indicated that EFA+CLA supplementation altered the proteome profile of the liver in transition dairy cows. Bioinformatics analysis of DAP revealed enriched pathways related to hepatic cholesterol biosynthesis, drug metabolism - cytochrome P450, metabolism of xenobiotics by cytochrome P450, chemical carcinogenesis, arachidonic acid metabolism, TCA cycle, and BA synthesis. Furthermore, in each time point, the relative abundance of CYP enzymes affected by EFA+CLA supplementation in a time-dependant manner slightly impacted the capacity of hepatic ω-oxidation. The results also suggest that EFA+CLA supplementation might be in support of preventing hepatic steatosis during the transition period. Altogether, these findings provided novel information regarding the underlying molecular mechanism by which hepatic metabolism responds to supplemented FA. Nonetheless, further investigation with more accurate measures of hepatic steatosis is needed to replicate these findings in different populations and physiological statuses.

Funding

This project has received funding from the European Union's Horizon 2020 research and innovation programme H2020-MSCA- ITN-2017- EJD: Marie Skłodowska-Curie Innovative Training Networks (European Joint Doctorate) – Grant agreement nº: 765423. The animal study was supported by BASF SE (Ludwigshafen, Germany).

Acknowledgements

The authors acknowledge A. Delavaud (INRAE) for technical assistance in protein extraction, quantification, and concentration for mass spectrometry analyses.

Declaration of Competing Interest

Authors declare no conflict of interests.

Figures legends

Figure 1) Schematic diagram of the (A) study design, (B) proteomics workflow, and (C) bioinformatics pipeline. (A) Timeline of treatments supplementation (from -63d ante to +63d postpartum) and liver biopsy collection (-21 d, +1 d, +28 d, and +63 d relative to parturition). Bold lines indicate liver biopsy sampling time points. (B) Protein extraction, purification, reduction, alkylation, and digestion; peptides were analysed by high-resolution LC-MS/MS, (C) Peptides alignment (progenesis), and protein identification (mascot) procedure were performed by Progenesis software coupled with the Mascot search engine, statistical analysis was based on Partial least squares discriminant analysis (PLS-DA) merged with $P < 0.05$ and Fold change > 1.5, followed by bioinformatics analysis (protein-protein interaction and Gene Ontology (GO) enrichment analysis.

Figure 2) A. Partial least squares discriminant analysis (PLS-DA) score plot of CTRL (red squares) and EFA+CLA (green triangle) on day 21 antepartum. B. Volcano plot represents differentially abundant proteins between CTRL and EFA+CLA group, increased (top right) and decreased (top left) proteins were highlighted in red ($P<0.05$ and fold change>than 0.58 in a log scale that means a fold change of 1.3). C. Hierarchical clustering heat map analysis of differentially abundant proteins; Rows and columns are sorted by similarity as indicated by the left (proteins) and top (samples) dendrograms, red and green represent CTRL and EFA+CLA, respectively. D. Biological Process Ontology for the differentially abundant proteins (DAP). Fold enrichment (Bars, –log10 (adjusted P-value)) refers to the number of relevant gene names represented in each category relative to random expression of all genes in the *Bos taurus* genome. The line between pathways represents their dependence. E. KEGG pathways map of DAP. The colour of the nodes represents the –log10 (adjusted P-value); the size of the dots represents the number of DAP in the pathway. The line between pathways represents their dependence.

Figure 3) A. Partial least squares discriminant analysis (PLS-DA) score plot of CTRL (red squares) and EFA+CLA (green triangle) in day 1 of postpartum. B. Volcano plot represents differentially abundant proteins between CTRL and EFA+CLA group, increased (top right) and decreased (top left) proteins were highlighted in red ($P<0.05$ and fold change>1.5). C. Hierarchical clustering heat map analysis of differentially abundant proteins, Rows and columns are respectively sorted by similarity as indicated by the left (proteins) and top (samples) dendrograms, red and green represent CTRL and EFA+CLA, respectively. D. Reactome enrichment analysis (x-axis), fold enrichment (bars, left y-axis); the number of significant genes in each pathway (–log10, adjusted P-value) is represented by the lines on the right y-axis) represent. E. KEGG pathways map of differentially abundant proteins (DAP). The colour of the nodes represents the –log10 (adjusted P-value); the size of the dots represents the number of DAP in the pathway. The line between pathways represents their dependence.

Figure 4) A. Partial least squares discriminant analysis (PLS-DA) score plot of CTRL (red squares) and EFA+CLA (green triangle) in day 28 of postpartum. B. Volcano plot represents differentially abundant proteins between CTRL and EFA+CLA group, increased (top right) and decreased (top left) proteins were highlighted in red ($P<0.05$ and fold change>1.5). C. Hierarchical clustering heat map analysis of differentially abundant proteins, Rows and columns are respectively sorted by similarity as indicated by the left (proteins) and top (samples) dendrograms, red and green represent CTRL and EFA+CLA, respectively. D. Biological Process Ontology for the differentially abundant proteins (DAP). The fold enrichment (adjusted P-value) is coloured in red according to the degree of significance, refers to the number of relevant gene names represented in each category relative to random expression of all genes in the Bos taurus genome. The line between pathways represents their dependence. E. KEGG pathways map of DAP. The colour of the nodes represents the –log10 (adjusted P-value); the size of the dots represents the number of DAP in the pathway. The line between pathways represents their dependence.

Figure 5) A. Partial least squares discriminant analysis (PLS-DA) score plot of CTRL (red squares) and EFA+CLA (green triangle) in day 63 of postpartum. B. Volcano plot represents differentially abundant proteins between CTRL and EFA+CLA group, increased (top right) and decreased (top left) proteins were highlighted in red ($P<0.05$ and fold change>1.5). C. Hierarchical clustering heat map analysis of differentially abundant proteins, Rows and columns are respectively sorted by similarity as indicated by the left (proteins) and top (samples) dendrograms, red and green represent CTRL and EFA+CLA, respectively. D. Reactome enrichment analysis (x-axis), fold enrichment (bars, left y-axis); the number of significant genes in each pathway (–log10, adjusted P-value) is represented by the lines on the right y-axis) represent. E. KEGG pathways map of differentially abundant proteins (DAP). The colour of the nodes represents the –log10 (adjusted P-value); the size of the dots represents the number of DAP in the pathway. The line between pathways represents their dependence.

Figure 6) Venn diagram represent common and specific differentially abundant proteins identified in -21, +1, +28, and +63 days relative to parturition.

Table heading

Table 1. The differentially abundant proteins identified between CTRL and EFA+CLA in -21, +1, +28, and +63 days relative to parturition and their associated gene names.

Num.	Protein	Associated gene name	Time point
1	20-beta-hydroxysteroid dehydrogenase-like	MGC127133	1, 2, 3, 4*
2	Progestagen Associated Endometrial Protein	PAEP	1, 2, 3, 4
3	Dimethylaniline monooxygenase [N-oxide-forming]	FMO5	1, 2, 3, 4
4	Immunoglobulin Lambda Like Polypeptide 5	IGLL5	1, 2, 3, 4
5	UDP-glucuronosyltransferase	UGT1A1	1, 2, 3, 4
6	Membrane bound O-acyltransferase domain containing 2	MBOAT2	1, 2, 4
7	Gamma-glutamylaminecyclotransferase	GGACT	2, 3, 4
8	Nicotinate phosphoribosyltransferase	NAPRT	1, 4
9	Beta-ureidopropionase 1	UPB1	2, 4
10	Glutamate-cysteine ligase catalytic subunit	GCLC	3, 4
11	Glutaminase 2	GLS2	3, 4
12	Calpain-2 catalytic subunit	CAPN2	3, 4
13	Calpastatin	CAST	3, 4
14	BoLA-DR-alpha	BoLA-DRA	3, 4
15	Prosaposin	PSAP	3, 4
16	Hydroxysteroid 11-beta dehydrogenase 1	HSD11B1	3, 4
17	Squalene epoxidase	SQLE	1
18	FDFT1 protein	FDFT1	1
19	Lanosterol 14-alpha demethylase	CYP51A1	1
20	Cytochrome P450 4A25-like	LOC784417	1
21	Inter-Alpha-Trypsin Inhibitor Heavy Chain 2	ITIH2	1
22	Peptidylprolyl Isomerase A	PPIA	1
23	Aldo-keto reductase family 1, member C5	AKR1C5	1
24	Putative glycerol kinase 5	GK5	1
25	Shootin 1	SHTN1	1
26	RNA Transcription, Translation And Transport Factor	RTRAF	1
27	Inter-alpha-trypsin inhibitor heavy chain H1	ITIH1	1
28	EF-hand domain-containing protein D2	EFHD2	1
29	Nucleoside diphosphate kinase	NME3	1
30	Aldo_ket_red domain-containing protein	LOC788425	1
31	Melanoma inhibitory activity protein 2	MIA2	1
32	RNA-binding protein 14	RBM14	1
33	Rab GDP dissociation inhibitor	GDI2	1
34	Ribosomal Protein S14	RPS14	1
35	Hydroxyacid-oxoacid transhydrogenase, mitochondrial	ADHFE1	1
36	Collagen Type X Alpha 1 Chain	COL10A1	1
37	Ras-related protein Rab-10	RAB10	1
38	Cingulin like 1	CGNL1	1
39	Legumain	LGMN	2

40	Tyrosine aminotransferase	TAT	2
41	Mannose-6-phosphate isomerase	MPI	2
42	Carboxylic ester hydrolase	BREH1	2
43	Cytochrome P450 Family 1 Subfamily A Polypeptide 1	CYP1A1	3
44	Ferritin light chain	FTL	3
45	Mediator Of Cell Motility 1	MEMO1	3
46	Ferritin	FTH1	3
47	Cathepsin C	CTSC	3
48	Heme oxygenase 1	HMOX1	3
49	Fatty acid amide hydrolase	FAAH	3
50	Thioesterase Superfamily Member 4	THEM4	3
51	Cytochrome P450 Family 4 Subfamily F Member 2	CYP4F2	3
52	Cytokine Induced Apoptosis Inhibitor 1	CIAPIN1	3
53	Reticulon-4-interacting protein 1, mitochondrial	RTN4IP1	3
54	Stomatin (EPB72)-like 2	STOML2	3
55	Queuosine salvage protein	C8H9orf64	3
56	Glutathione S-transferase Mu 1	GSTM4	3
57	Acyl-CoA synthetase short chain family member 2	ACSS2	4
58	Pyridoxal phosphate phosphatase	PDXP	4
59	Histidine ammonia-lyase	HAL	4
60	D-amino acid oxidase	DAO	4
61	Cytochrome P450 Family 4 Subfamily V Member 2	CYP4V2	4
62	High Mobility Group Box 2	HMGB2	4
63	Indoleamine 2,3-dioxygenase 2	IDO2	4
64	Decorin	DCN	4
65	Heterogeneous nuclear ribonucleoprotein D	HNRNPD	4
66	Asparaginase And Isoaspartyl Peptidase 1	ASRGL1	4
67	VPS35 Retromer Complex Component	VPS35	4

*1, 2, 3, and 4 correspond to days -21, +1, +28, and +63 relative to parturition, respectively.

Supplementary Material

Supplementary S1

Table S1. Amounts of daily abomasally infused supplements[1].

Supplementation	treatment			
	CTRL[2]	EFA+CLA		
	Coconut oil[3]	Linseed oil[4]	Safflower oil[5]	Lutalin®[6]
Daily infused oils (g/d)				
Dosage lactation	76	78	4	38
Dosage dry period	38	39	2	19
Daily infused fatty acids (g/d) at the lactation dosage[7]				
18:3 cis-9, cis-12, cis-15	0.00	39.9	0.01	0.00
18:2 cis-9, cis-12	1.39	12.4	2.48	1.34
18:2 cis-9, trans-11	0.00	0.00	0.01	10.3
18:2 trans-10, cis-12	0.00	0.02	0.01	10.2

1Cows were supplemented daily with coconut oil (CTRL), or a mixture of linseed, safflower oil (EFA), and Lutalin® (CLA, c9, t11 and t10, c12), (EFA+CLA).
2Addition of vitamin E (0.06 g/d), Covitol 1360 (BASF, Ludwigshafen, Germany), to compensate for the vitamin E in linseed oil (0.07%) and safflower oil (0.035%).
3Sanct Bernhard, Bad Ditzenbach, Germany
4DERBY, Derby Spezialfutter GmbH, Münster, Germany
5GEFRO, Memmingen/Allgäu, Germany
6BASF, Ludwigshafen, Germany
7The lactation dosage was halved during the dry period.

Supplementary S2

Table S2. Ingredients and chemical compositions of the diets.

Item (g/kg of DM)	Diet	
	Dry period[1]	Lactation
Ingredients	421	457
Corn silage Straw	223	97
Compound feed DEFA[2] (granulated)	-	446
Dried sugar beet pulp	163	-
Extracted soybean meal	99	-
Grain of rye	75	-
Mineral-vitamin mixture[3]	10	-
Urea[4]	9	-
Chemical composition		
NEL (MJ/kg DM)[5]	6.2	7.1
Crude fat	21	23
Crude fiber	219	173
Crude protein	141	146
Utilizable protein[5]	141	143
NFC	379	432
NDF	423	346
ADF	249	197
RNB[5,6]	0.0	0.5

[1] The dry period diet was fed from wk 6 to wk 1 before calving.
[2] Ceravis AG, Malchin, Germany Ingredients: 46.5% dried sugar beet pulp, 25.3% extracted soybean meal, 23.8% grain of rye, 1.4% urea, 1.1% premix cow, 1.00% calcium, 0.37% phosphorus, 0.42% sodium, vitamins A, D3, E, copper, ferric, zinc, manganese, cobalt, iodine, selenium Chemical composition: 44.4% NFC, 24.1% crude protein, 21.6% NDF, 12.4% ADF, 9.3% crude fiber, 8.2% crude ash, 1.8% crude fat, 7.9 MJ NEL/kg DM
[3] KULMIN®MFV Plus (Bergophor Futtermittelfabrik Dr. Berger GmbH & Co. KG, Kulmbach, Germany): 8.5% magnesium, 7.5% phosphorus, 6.5% sodium, 3.5% HCl insoluble ash, 1.5% calcium, additives: vitamins A, D3, E, B1, B2, B6, B5, B3, B12, B9, H, zinc, manganese, copper, cobalt, iodine, selenium, and Saccharomyces cerevisiae
[4] Piarumin® (SKW Stickstoffwerke Piesteritz GmbH, Lutherstadt Wittenberg, Germany): 99% urea, 46.5% total nitrogen
[5] Society of Nutrition Physiology (GfE, 2001, 2008, 2009) and Deutsche Landwirtschaftliche Gesellschaft (DLG, 2013)
[6] RNB = ruminal nitrogen balance

Supplementary S3.

Table S3. Performance data of day 21 ante, and days +1, +28, and +63 postpartum of cows supplemented abomasally with coconut oil (CTRL; n = 8), or the combination of linseed and safflower oil (EFA) and conjugated linoleic acid (CLA) (EFA+CLA; n=8) from wk 9 antepartum until wk 9 postpartum, Adapted from [11].

		treatment		Fixed effect, P-value		
		CTRL	EFA+ CLA	EFA+ CLA	time	EFA+CLA*time
NEL intake, MJ NEL/d	late lactation	120.2 ± 4.6	113.8 ± 3.9	0.7	0.12	
	Dry period	80.6 ± 3.1	84.1 ± 2.8	0.8	0.001	
	Transition period	93.9 ± 3.3	93.4 ± 2.9	0.7	0.001	
	Postpartum	120.8 ± 3.8	115 ± 3.5	0.3	0.001	
	Entire Study	106.6 ± 3.3	104 ± 2.9	0.6	0.001	
FEMY, kg milk/kg DMI	late lactation	0.96 ± 0.11	0.98 ± 0.09	0.19	0.001	
	Early lactation	2.25 ± 0.1	2.43 ± 0.09	0.7	0.001	
FEECM, kg ECM/kg DMI	late lactation	1.08 ± 0.1	0.95 ± 0.09	0.2	0.001	
	Early lactation	2.31 ± 0.11	1.95 ± 0.1	0.5	0.001	
BW, kg	late lactation	701 ± 21	670 ± 19	0.5	0.001	
	Dry period	742 ± 22	718 ± 20	0.2	0.001	
	Transition period	690 ± 20	672 ± 18	0.3	0.001	
	Postpartum	634 ± 18	621 ± 17	0.4	0.001	
	Entire Study	685 ± 20	665 ± 18	0.3	0.001	
BCS	late lactation	3.62 ± 0.11	3.29 ± 0.1	0.7	0.001	
	Dry period	3.72 ± 0.12	3.62 ± 0.11	0.9	0.001	
	Transition period	3.54 ± 0.12	3.5 ± 0.11	1	0.001	
	Postpartum	3.12 ± 0.11	3.1 ± 0.1	0.8	0.001	
	Entire Study	3.43 ± 0.11	3.31 ± 0.1	0.8	0.001	
BFT, mm	late lactation	13.4 ± 1	11.3 ± 0.9	0.8	0.001	
	Dry period	15.3 ± 1.1	14.6 ± 1	0.9	0.001	
	Transition period	14.7 ± 1.1	14.5 ± 1	0.8	0.001	
	Postpartum	12.1 ± 1	12.6 ± 0.9	0.8	0.001	
	Entire Study	13.5 ± 1	13 ± 0.9	0.9	0.001	

1Values are presented as the LSM ± SE.
2FEMY = feed efficiency for milk production; FEECM = feed efficiency for ECM production; BFT = back fat thickness.

Supplementary S4.

Plasma concentrations of (A) non-esterified fatty acids (NEFA), (B) β-hydroxybutyrate (BHB), (C) triglycerides, (D) low-density lipoprotein (LDL), (E) total cholesterol, (F) high-density lipoprotein (HDL), (G) haptoglobin, and (H) paraxonase from 83 d before until 63 d after calving in cows supplemented daily with coconut oil (○ CTRL; n = 8), or a combination of linseed and safflower oil and Lutalin (cis-9,trans-11 and trans-10,cis-12 CLA; BASF, Ludwigshafen, Germany; ◆EFA+CLA; n = 8). Changes in plasma metabolites concentrations were analyzed using the MIXED procedure by repeated-measures ANOVA. Data are presented as the least squares means (LSM) and their standard errors (SE) (LSM ± SE), LSM with different superscripts (a, b) differ (P < 0.05) at the respective time point. Statistically significant (P < 0.05) effects for (A) NEFA concentration during the entire study (time; EFA+CLA × time interaction). Statistically significant (P < 0.05) effect for (B) BHB, (C) triglycerides, (D) LDL, (E) total cholesterol, (F) HDL, (G) haptoglobin, and (H) paraxonase concentration during the time. Adapted from [11, 16, 17].

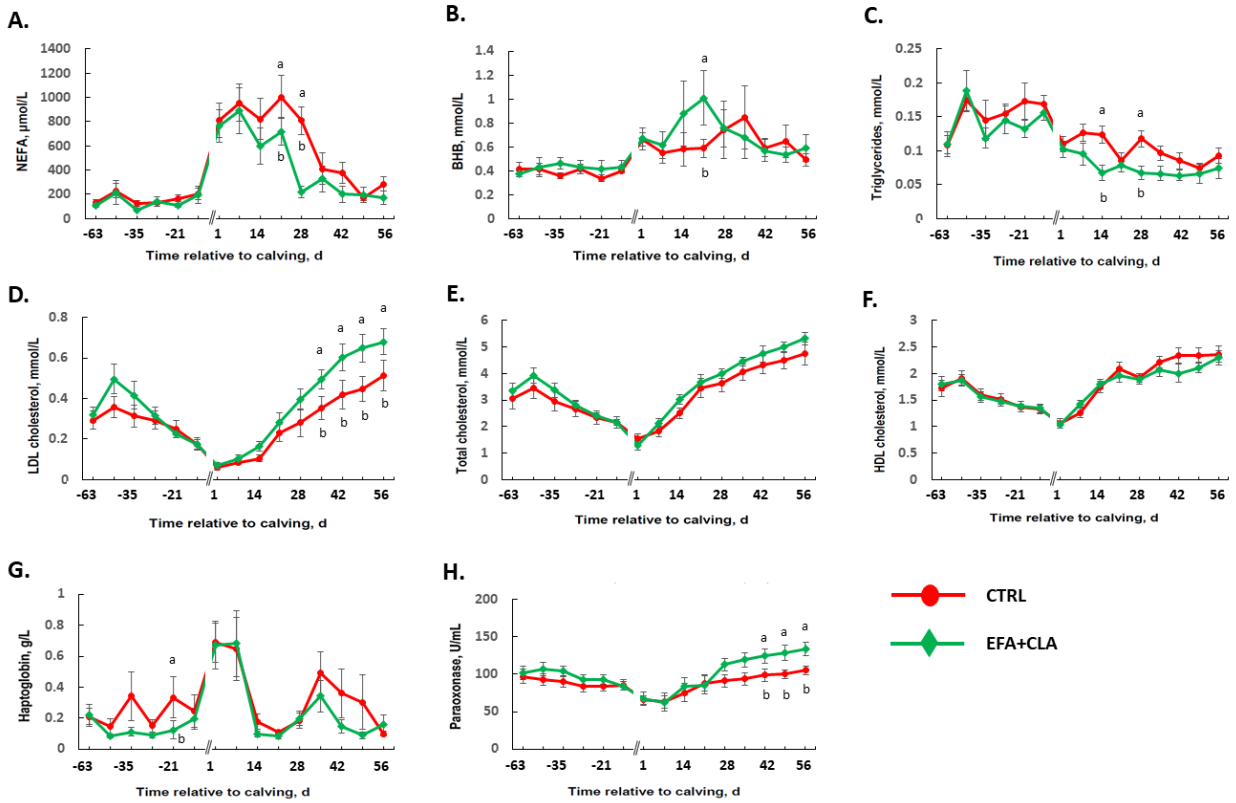

Supplementary files

The data and related analyses are available through the link https://doi.org/10.15454/5U5WQS.

Reference

[1] Y. Shen, L. Chen, W. Yang, Z. Wang, Exploration of serum sensitive biomarkers of fatty liver in dairy cows, sci, Rep. 8(1) (2018) 13574.

662 [2] B. Moran, S.B. Cummins, C.J. Creevey, S.T. Butler, Transcriptomics of liver and muscle in Holstein
663 cows genetically divergent for fertility highlight differences in nutrient partitioning and inflammation
664 processes, BMC Genomics 17(1) (2016) 603.

665 [3] P. Li, Y. Liu, Y. Zhang, M. Long, Y. Guo, Z. Wang, X. Li, C. Zhang, X. Li, J. He, G. Liu, Effect of Non-
666 Esterified Fatty Acids on Fatty Acid Metabolism-Related Genes in Calf Hepatocytes Cultured in Vitro,
667 Cell. Physiol. Biochem. 32(5) (2013) 1509-1516.

668 [4] R.A. Vaughan, R. Garcia-Smith, M. Bisoffi, C.A. Conn, K.A. Trujillo, Conjugated linoleic acid or omega 3
669 fatty acids increase mitochondrial biosynthesis and metabolism in skeletal muscle cells, Lipids Health Dis
670 11 (2012) 142.

671 [5] J.A.A. Pires, R.R. Grummer, Specific fatty acids as metabolic modulators in the dairy cow, Rev Bras
672 Zootec 37 (2008) 287-298.

673 [6] M. Hussein, K.H. Harvatine, W.M. Weerasinghe, L.A. Sinclair, D.E. Bauman, Conjugated linoleic acid-
674 induced milk fat depression in lactating ewes is accompanied by reduced expression of mammary genes
675 involved in lipid synthesis, J Dairy Sci 96(6) (2013) 3825-34.

676 [7] A. Suárez-Vega, B. Gutiérrez-Gil, P.G. Toral, G. Hervás, J.J. Arranz, P. Frutos, Conjugated linoleic acid
677 (CLA)-induced milk fat depression: application of RNA-Seq technology to elucidate mammary gene
678 regulation in dairy ewes, Sci, Rep. 9(1) (2019) 4473.

679 [8] E. Bichi, G. Hervas, P.G. Toral, J.J. Loor, P. Frutos, Milk fat depression induced by dietary marine algae
680 in dairy ewes: persistency of milk fatty acid composition and animal performance responses, J Dairy Sci
681 96(1) (2013) 524-32.

682 [9] K.J. Harvatine, J.W. Perfield, 2nd, D.E. Bauman, Expression of enzymes and key regulators of lipid
683 synthesis is upregulated in adipose tissue during CLA-induced milk fat depression in dairy cows, J Nutr
684 139(5) (2009) 849-54.

685 [10] B.J. Thering, D.E. Graugnard, P. Piantoni, J.J. Loor, Adipose tissue lipogenic gene networks due to
686 lipid feeding and milk fat depression in lactating cows, J Dairy Sci 92(9) (2009) 4290-300.

687 [11] L. Vogel, M. Gnott, C. Kroger-Koch, D. Dannenberger, A. Tuchscherer, A. Troscher, H. Kienberger, M.
688 Rychlik, A. Starke, L. Bachmann, H.M. Hammon, Effects of abomasal infusion of essential fatty acids
689 together with conjugated linoleic acid in late and early lactation on performance, milk and body
690 composition, and plasma metabolites in dairy cows, J Dairy Sci 103(8) (2020) 7431-7450.

691 [12] R. Mohammed, C.S. Stanton, J.J. Kennelly, J.K. Kramer, J.F. Mee, D.R. Glimm, M. O'Donovan, J.J.
692 Murphy, Grazing cows are more efficient than zero-grazed and grass silage-fed cows in milk rumenic
693 acid production, J Dairy Sci 92(8) (2009) 3874-93.

694 [13] L. Bernard, M. Bonnet, C. Delavaud, M. Delosière, A. Ferlay, H. Fougère, B. Graulet, Milk Fat Globule
695 in Ruminant: Major and Minor Compounds, Nutritional Regulation and Differences Among Species, Eur.
696 J. Lipid Sci. Technol. 120(5) (2018) 1700039.

697 [14] P. Gómez-Cortés, P. Frutos, A.R. Mantecón, M. Juárez, M.A. de la Fuente, G. Hervás, Effect of
698 supplementation of grazing dairy ewes with a cereal concentrate on animal performance and milk fatty
699 acid profile, J Dairy Sci 92(8) (2009) 3964-72.

[15] S.L. White, J.A. Bertrand, M.R. Wade, S.P. Washburn, J.T. Green, Jr., T.C. Jenkins, Comparison of fatty acid content of milk from Jersey and Holstein cows consuming pasture or a total mixed ration, J Dairy Sci 84(10) (2001) 2295-301.

[16] M. Gnott, L. Vogel, C. Kroger-Koch, D. Dannenberger, A. Tuchscherer, A. Troscher, E. Trevisi, T. Stefaniak, J. Bajzert, A. Starke, M. Mielenz, L. Bachmann, H.M. Hammon, Changes in fatty acids in plasma and association with the inflammatory response in dairy cows abomasally infused with essential fatty acids and conjugated linoleic acid during late and early lactation, J Dairy Sci (2020).

[17] L. Vogel, M. Gnott, C. Kroger-Koch, S. Gors, J.M. Weitzel, E. Kanitz, A. Hoeflich, A. Tuchscherer, A. Troscher, J.J. Gross, R.M. Bruckmaier, A. Starke, L. Bachmann, H.M. Hammon, Glucose metabolism and the somatotropic axis in dairy cows after abomasal infusion of essential fatty acids together with conjugated linoleic acid during late gestation and early lactation, J Dairy Sci 104(3) (2021) 3646-3664.

[18] J.R. Yates, 3rd, Recent technical advances in proteomics, F1000Res 8 (2019) F1000 Faculty Rev-351.

[19] D. Veyel, K. Wenger, A. Broermann, T. Bretschneider, A.H. Luippold, B. Krawczyk, W. Rist, E. Simon, Biomarker discovery for chronic liver diseases by multi-omics – a preclinical case study, Sci, Rep. 10(1) (2020) 1314.

[20] L.D. Fonseca, J.P. Eler, M.A. Pereira, A.F. Rosa, P.A. Alexandre, C.T. Moncau, F. Salvato, L. Rosa-Fernandes, G. Palmisano, J.B.S. Ferraz, H. Fukumasu, Liver proteomics unravel the metabolic pathways related to Feed Efficiency in beef cattle, Sci Rep 9(1) (2019) 5364.

[21] H. Sejersen, M.T. Sorensen, T. Larsen, E. Bendixen, K.L. Ingvartsen, Liver protein expression in dairy cows with high liver triglycerides in early lactation, J Dairy Sci 95(5) (2012) 2409-21.

[22] L. Ma, Y. Yang, X. Zhao, F. Wang, S. Gao, D. Bu, Heat stress induces proteomic changes in the liver and mammary tissue of dairy cows independent of feed intake: An iTRAQ study, PLoS One 14(1) (2019) e0209182.

[23] A.L. Skibiel, M. Zachut, B.C. do Amaral, Y. Levin, G.E. Dahl, Liver proteomic analysis of postpartum Holstein cows exposed to heat stress or cooling conditions during the dry period, J Dairy Sci 101(1) (2018) 705-716.

[24] GfE; Gesellschaft für Ernährungsphysiologie (German Society of Nutrition Physiology). 2001. Empfehlungen zur Energie- und Nährstoffversorgung der Milchkühe und Aufzuchtrinder (Recommended energy and nutrient suply of dairy cows and growing cattle). Vol. 8. DLGVerlag, Frankfurt a. M., Germany.

[25] GfE; Gesellschaft für Ernährungsphysiologie (German Society of Nutrition Physiology). 2008. New equations for predicting metabolisable energy of grass and maize products for ruminants. Communications of the Committee for Requirement Standards of the Society of Nutrition Physiology. Proc. Soc. Nutr. Physiol. 17:191–198.

[26] GfE; Gesellschaft für Ernährungsphysiologie (German Society of Nutrition Physiology). 2009. New equations for predicting metabolisable energy of compound feeds for cattle. Communications of the Committee for Requirement Standards of the Society of Nutrition Physiology. Proc. Soc. Nutr. Physiol. 18:143–146.

[27] DLG (Deutsche Landwirtschafts-Gesellschaft, German Agricultural Society). 2013. Leitfaden zur Berechnung des Energiegehaltes bei Einzel-und Mischfuttermitteln für die Schweine-und

Rinderfütterung (Guidelines for calculation of energy content of single and mixed feedstuff for pigs and cattle). Stellungnahme des DLG-Arbeitskreises Futter und Fütterung.

[28] C. Weber, C. Hametner, A. Tuchscherer, B. Losand, E. Kanitz, W. Otten, S.P. Singh, R.M. Bruckmaier, F. Becker, W. Kanitz, H.M. Hammon, Variation in fat mobilization during early lactation differently affects feed intake, body condition, and lipid and glucose metabolism in high-yielding dairy cows, J Dairy Sci 96(1) (2013) 165-80.

[29] T. Santos, D. Viala, C. Chambon, J. Esbelin, M. Hebraud, Listeria monocytogenes Biofilm Adaptation to Different Temperatures Seen Through Shotgun Proteomics, Front Nutr 6 (2019) 89.

[30] J. Bazile, B. Picard, C. Chambon, A. Valais, M. Bonnet, Pathways and biomarkers of marbling and carcass fat deposition in bovine revealed by a combination of gel-based and gel-free proteomic analyses, Meat sci 156 (2019) 146-155.

[31] A. Veshkini, Gene ontology of hepatic differentially abundant proteins in Holstein cows supplemented with essential fatty acids and conjugated linoleic acids, Portail Data INRAE, 2021. https://doi.org/10.15454/5U5WQS.

[32] D.W. Nebert, K. Wikvall, W.L. Miller, Human cytochromes P450 in health and disease, Philos. Trans. Roy. Soc. B: Biol. Sci. 368 368(1612) (2013) 20120431.

[33] E. Stavropoulou, G.G. Pircalabioru, E. Bezirtzoglou, The Role of Cytochromes P450 in Infection, Front in Immunol 9(89) (2018).

[34] R.J.A. Wanders, J. Komen, S. Kemp, Fatty acid omega-oxidation as a rescue pathway for fatty acid oxidation disorders in humans, The FEBS J. 278(2) (2011) 182-194.

[35] Y. Miura, The biological significance of ω-oxidation of fatty acids, Proceedings of the Jpn Acad. Ser. B. Phys. Biol. Sci. 89(8) (2013) 370-382.

[36] I. Elfaki, R. Mir, F.M. Almutairi, F.M.A. Duhier, Cytochrome P450: Polymorphisms and Roles in Cancer, Diabetes and Atherosclerosis, Asian Pac J Cancer Prev 19(8) (2018) 2057-2070.

[37] V.Y. Ng, Y. Huang, L.M. Reddy, J.R. Falck, E.T. Lin, D.L. Kroetz, Cytochrome P450 eicosanoids are activators of peroxisome proliferator-activated receptor alpha, Drug Metab Dispos 35(7) (2007) 1126-34.

[38] Y.M. Wang, S.S. Ong, S.C. Chai, T. Chen, Role of CAR and PXR in xenobiotic sensing and metabolism, Expert Opin Drug Metab Toxicol 8(7) (2012) 803-17.

[39] A.D. Patterson, F.J. Gonzalez, J.R. Idle, Xenobiotic metabolism: a view through the metabolometer, Chem. Res. Toxicol. 23(5) (2010) 851-860.

[40] N.C. Sadler, B.-J.M. Webb-Robertson, T.R. Clauss, J.G. Pounds, R. Corley, A.T. Wright, High-Fat Diets Alter the Modulatory Effects of Xenobiotics on Cytochrome P450 Activities, Chem Res Toxicol 31(5) (2018) 308-318.

[41] F. Scott, S.G. Gonzalez Malagon, B.A. O'Brien, D. Fennema, S. Veeravalli, C.R. Coveney, I.R. Phillips, E.A. Shephard, Identification of Flavin-Containing Monooxygenase 5 (FMO5) as a Regulator of Glucose Homeostasis and a Potential Sensor of Gut Bacteria, Drug Metab. Dispos. 45(9) (2017) 982-989.

[42] S.G. Gonzalez Malagon, A.N. Melidoni, D. Hernandez, B.A. Omar, L. Houseman, S. Veeravalli, F. Scott, D. Varshavi, J. Everett, Y. Tsuchiya, J.F. Timms, I.R. Phillips, E.A. Shephard, The phenotype of a

knockout mouse identifies flavin-containing monooxygenase 5 (FMO5) as a regulator of metabolic ageing, Biochem. Pharmacol. 96(3) (2015) 267-277.

[43] M. Lewinska, U. Zelenko, F. Merzel, S. Golic Grdadolnik, J.C. Murray, D. Rozman, Polymorphisms of CYP51A1 from cholesterol synthesis: associations with birth weight and maternal lipid levels and impact on CYP51 protein structure, PLoS One 8(12) (2013) e82554.

[44] A. Kondo, S. Yamamoto, R. Nakaki, T. Shimamura, T. Hamakubo, J. Sakai, T. Kodama, T. Yoshida, H. Aburatani, T. Osawa, Extracellular Acidic pH Activates the Sterol Regulatory Element-Binding Protein 2 to Promote Tumor Progression, Cell Rep 18(9) (2017) 2228-2242.

[45] L. Chen, M.-Y. Ma, M. Sun, L.-Y. Jiang, X.-T. Zhao, X.-X. Fang, S. Man Lam, G.-H. Shui, J. Luo, X.-J. Shi, B.-L. Song, Endogenous sterol intermediates of the mevalonate pathway regulate HMGCR degradation and SREBP-2 processing[S], J. Lipid Res. 60(10) (2019) 1765-1775.

[46] J. Grünler, J. Ericsson, G. Dallner, Branch-point reactions in the biosynthesis of cholesterol, dolichol, ubiquinone and prenylated proteins, Biochim Biophys Acta 1212(3) (1994) 259-77.

[47] L. Xue, H. Qi, H. Zhang, L. Ding, Q. Huang, D. Zhao, B.J. Wu, X. Li, Targeting SREBP-2-Regulated Mevalonate Metabolism for Cancer Therapy, Front Oncol 10 (2020) 1510-1510.

[48] W. Eid, K. Dauner, K.C. Courtney, A. Gagnon, R.J. Parks, A. Sorisky, X. Zha, mTORC1 activates SREBP-2 by suppressing cholesterol trafficking to lysosomes in mammalian cells, Proceed. Nat. Acad. Sci. 114(30) (2017) 7999-8004.

[49] Y. Zhang, S.R. Breevoort, J. Angdisen, M. Fu, D.R. Schmidt, S.R. Holmstrom, S.A. Kliewer, D.J. Mangelsdorf, I.G. Schulman, Liver LXRα expression is crucial for whole body cholesterol homeostasis and reverse cholesterol transport in mice, J. Clin Invest. 122(5) (2012) 1688-99.

[50] H. Akamatsu, Y. Saitoh, M. Serizawa, K. Miyake, Y. Ohba, K. Nakashima, Changes of serum 3-methylhistidine concentration and energy-associated metabolites in dairy cows with ketosis, J Vet Med Sci 69(10) (2007) 1091-3.

[51] H. Shimano, SREBPs: physiology and pathophysiology of the SREBP family, The FEBS J. 276(3) (2009) 616-621.

[52] L. Woollett, Review: Transport of Maternal Cholesterol to the Fetal Circulation, Placenta 32 Suppl 2 (2011) S218-21.

[53] Y. Wang, W.-X. Ding, T. Li, Cholesterol and bile acid-mediated regulation of autophagy in fatty liver diseases and atherosclerosis, Biochim Biophys Acta Mol Cell Biol Lipids 1863(7) (2018) 726-733.

[54] H.U. Marschall, Management of intrahepatic cholestasis of pregnancy, Expert Rev. Gastroenterol. Hepatol. 9(10) (2015) 1273-9.

[55] H. Shindou, D. Hishikawa, T. Harayama, K. Yuki, T. Shimizu, Recent progress on acyl CoA: lysophospholipid acyltransferase research, J. Lipid Res. 50 Suppl(Suppl) (2009) S46-S51.

[56] M. Eto, H. Shindou, S. Yamamoto, M. Tamura-Nakano, T. Shimizu, Lysophosphatidylethanolamine acyltransferase 2 (LPEAT2) incorporates DHA into phospholipids and has possible functions for fatty acid-induced cell death, Biochem. Biophys. Res. Commun. 526(1) (2020) 246-252.

[57] V. Malagnino, J. Hussner, A. Issa, A. Midzic, H.E. Meyer Zu Schwabedissen, OATP1B3-1B7, a novel organic anion transporting polypeptide, is modulated by FXR ligands and transports bile acids, Am. J. Physiol. Gastrointest. Liver Physiol. 317(6) (2019) G751-g762.

[58] B. Hagenbuch, C. Gui, Xenobiotic transporters of the human organic anion transporting polypeptides (OATP) family, Xenobiotica; the fate of foreign comp Biol. Syst. 38 (2008) 778-801.

[59] P. Pathak, H. Liu, S. Boehme, C. Xie, K.W. Krausz, F. Gonzalez, J.Y.L. Chiang, Farnesoid X receptor induces Takeda G-protein receptor 5 cross-talk to regulate bile acid synthesis and hepatic metabolism, J. Biol Chem. 292(26) (2017) 11055-11069.

[60] H. Hao, L. Cao, C. Jiang, Y. Che, S. Zhang, S. Takahashi, G. Wang, F.J. Gonzalez, Farnesoid X Receptor Regulation of the NLRP3 Inflammasome Underlies Cholestasis-Associated Sepsis, Cell Metab 25(4) (2017) 856-867.e5.

[61] C. Guo, S. Xie, Z. Chi, J. Zhang, Y. Liu, L. Zhang, M. Zheng, X. Zhang, D. Xia, Y. Ke, L. Lu, D. Wang, Bile Acids Control Inflammation and Metabolic Disorder through Inhibition of NLRP3 Inflammasome, Immunity 45(4) (2016) 802-816.

[62] M. McCabe, S. Waters, D. Morris, D. Kenny, D. Lynn, C. Creevey, RNA-seq analysis of differential gene expression in liver from lactating dairy cows divergent in negative energy balance, BMC Genomics 13 (2012) 193.

[63] G. Kakiyama, D. Marques, H. Takei, H. Nittono, S. Erickson, M. Fuchs, D. Rodriguez-Agudo, G. Gil, P.B. Hylemon, H. Zhou, J.S. Bajaj, W.M. Pandak, Mitochondrial oxysterol biosynthetic pathway gives evidence for CYP7B1 as controller of regulatory oxysterols, J. Steroid Biochem. Mol. Biol. 189 (2019) 36-47.

[64] D. Bartolini, P. Torquato, C. Barola, A. Russo, C. Rychlicki, D. Giusepponi, G. Bellezza, A. Sidoni, R. Galarini, G. Svegliati-Baroni, F. Galli, Nonalcoholic fatty liver disease impairs the cytochrome P-450-dependent metabolism of α-tocopherol (vitamin E), J. Nutr. Biochem. 47 (2017) 120-131.

[65] Y.B. Jarrar, S.-J. Lee, Molecular Functionality of Cytochrome P450 4 (CYP4) Genetic Polymorphisms and Their Clinical Implications, Int. J. Mol. Sci. 20(17) (2019) 4274.

[66] X. Cui, D.R. Nelson, H.W. Strobel, A novel human cytochrome P450 4F isoform (CYP4F11): cDNA cloning, expression, and genomic structural characterization, Genomics 68(2) (2000) 161-6.

[67] M. Nakano, E.J. Kelly, C. Wiek, H. Hanenberg, A.E. Rettie, CYP4V2 in Bietti's crystalline dystrophy: ocular localization, metabolism of ω-3-polyunsaturated fatty acids, and functional deficit of the p.H331P variant, Mol Pharmacol 82(4) (2012) 679-686.

[68] K.Z. Edson, B. Prasad, J.D. Unadkat, Y. Suhara, T. Okano, F.P. Guengerich, A.E. Rettie, Cytochrome P450-dependent catabolism of vitamin K: ω-hydroxylation catalyzed by human CYP4F2 and CYP4F11, Biochemistry 52(46) (2013) 8276-8285.

[69] Y.B. Jarrar, S.A. Cho, K.S. Oh, D.H. Kim, J.G. Shin, S.J. Lee, Identification of cytochrome P450s involved in the metabolism of arachidonic acid in human platelets, Prostaglandins, leukot, Essent. Fat. Acids, 89(4) (2013) 227-34.

[70] J.M. Weinberg, Lipotoxicity, Kidney int. 70(9) (2006) 1560-6.

853 [71] M.H. Hsu, U. Savas, J.M. Lasker, E.F. Johnson, Genistein, resveratrol, and 5-aminoimidazole-4-
854 carboxamide-1-beta-D-ribofuranoside induce cytochrome P450 4F2 expression through an AMP-
855 activated protein kinase-dependent pathway, J Pharmacol Exp Ther 337(1) (2011) 125-36.

856 [72] J. Lu, X. Shang, W. Zhong, Y. Xu, R. Shi, X. Wang, New insights of CYP1A in endogenous metabolism:
857 a focus on single nucleotide polymorphisms and diseases, Acta Pharm. Sin. B 10(1) (2020) 91-104.

858 [73] R. Santes-Palacios, D. Ornelas-Ayala, N. Cabañas, A. Marroquín-Pérez, A. Hernández-Magaña, S. del
859 Rosario Olguín-Reyes, R. Camacho-Carranza, J.J. Espinosa-Aguirre, Regulation of Human Cytochrome
860 P4501A1 (hCYP1A1): A Plausible Target for Chemoprevention?, Biomed. Res. Int. 2016 (2016) 5341081.

861 [74] S. Huerta-Yepez, A. Tirado-Rodriguez, M.R. Montecillo-Aguado, J. Yang, B.D. Hammock, O.
862 Hankinson, Aryl Hydrocarbon Receptor-Dependent inductions of omega-3 and omega-6 polyunsaturated
863 fatty acid metabolism act inversely on tumor progression, Sci Rep. 10(1) (2020) 7843.

864 [75] D. Choudhary, I. Jansson, I. Stoilov, M. Sarfarazi, J.B. Schenkman, METABOLISM OF RETINOIDS AND
865 ARACHIDONIC ACID BY HUMAN AND MOUSE CYTOCHROME P450 1B1, Drug Metab. Dispos. 32(8) (2004)
866 840.

867 [76] M. Fer, Y. Dréano, D. Lucas, L. Corcos, J.-P. Salaün, F. Berthou, Y. Amet, Metabolism of
868 eicosapentaenoic and docosahexaenoic acids by recombinant human cytochromes P450, Arch. Biochem.
869 Biophys. 471(2) (2008) 116-125.

870 [77] D. Schwarz, P. Kisselev, S.S. Ericksen, G.D. Szklarz, A. Chernogolov, H. Honeck, W.-H. Schunck, I.
871 Roots, Arachidonic and eicosapentaenoic acid metabolism by human CYP1A1: highly stereoselective
872 formation of 17(R),18(S)-epoxyeicosatetraenoic acid, Biochem. Pharmacol. 67(8) (2004) 1445-1457.

873 [78] K.S. Guruge, N. Yamanaka, J. Hasegawa, S. Miyazaki, Differential induction of cytochrome P450 1A1
874 and 1B1 mRNA in primary cultured bovine hepatocytes treated with TCDD, PBDD/Fs and feed
875 ingredients, Toxicol. Lett. 185(3) (2009) 193-196.

876 [79] B. Huang, J. Bao, Y.R. Cao, H.F. Gao, Y. Jin, Cytochrome P450 1A1 (CYP1A1) Catalyzes Lipid
877 Peroxidation of Oleic Acid-Induced HepG2 Cells, Biochemistry (Moscow) 83(5) (2018) 595-602.

878 [80] C. Shi, L. Min, J. Yang, M. Dai, D. Song, H. Hua, G. Xu, F.J. Gonzalez, A. Liu, Peroxisome Proliferator-
879 Activated Receptor α Activation Suppresses Cytochrome P450 Induction Potential in Mice Treated with
880 Gemfibrozil, Basic Clin. Pharmacol. Toxicol. 121(3) (2017) 169-174.

881 [81] S.D. Yelamanchi, S. Jayaram, J.K. Thomas, S. Gundimeda, A.A. Khan, A. Singhal, T.S. Keshava Prasad,
882 A. Pandey, B.L. Somani, H. Gowda, A pathway map of glutamate metabolism, J Cell Commun Signal 10(1)
883 (2016) 69-75.

884 [82] L. Han, F. Batistel, Y. Ma, A.S.M. Alharthi, C. Parys, J.J. Loor, Methionine supply alters mammary
885 gland antioxidant gene networks via phosphorylation of nuclear factor erythroid 2-like 2 (NFE2L2)
886 protein in dairy cows during the periparturient period, J. Dairy Sci. 101(9) (2018) 8505-8512.

887 [83] D. Yang, H. Brunengraber, Glutamate, a window on liver intermediary metabolism, J Nutr 130(4S
888 Suppl) (2000) 991s-4s.

889 [84] A.J. Meijer, Amino acids as regulators and components of nonproteinogenic pathways, J Nutr 133(6
890 Suppl 1) (2003) 2057s-2062s.

[85] H.Y. Kang, Y.-K. Choi, Y.I. Jeong, K.-C. Choi, S.-H. Hyun, W.-S. Hwang, E.-B. Jeung, Immortalization of Porcine 11β-Hydroxysteroid Dehydrogenase Type 1-Transgenic Liver Cells Using SV40 Large T Antigen, Int. J. Mol. Sci. 18(12) (2017) 2625.

[86] P. Huang, Y. Li, C. Xu, G. Melino, C. Shao, Y. Shi, HSD11B1 is upregulated synergistically by IFNγ and TNFα and mediates TSG-6 expression in human UC-MSCs, Cell Death Dis 6(1) (2020) 24.

[87] Y. Maeda, S. Naganuma, I. Niina, A. Shinohara, C. Koshimoto, K. Kondo, K. Chijiiwa, Effects of bile acids on rat hepatic microsomal type I 11β-hydroxysteroid dehydrogenase, Steroids 75(2) (2010) 164-168.

[88] M. Yi, J.G. Shin, S.J. Lee, Expression of CYP4V2 in human THP1 macrophages and its transcriptional regulation by peroxisome proliferator-activated receptor gamma, Toxicol. Appl. Pharmacol. 330 (2017) 100-106.

[89] M. Nakano, E. Kelly, A. Rettie, Expression and Characterization of CYP4V2 as a Fatty Acid -Hydroxylase, Drug Metab. Dispos.: Biol. Fate Chem. 37 (2009) 2119–2122.